11. Nakatsukasa E, Inomata T, Ikeda T, Shino M, Kashiwazaki N (2001) Generation of live rat offspring by intrauterine insemination with epididymal spermatozoa cryopreserved at −196°C. Reproduction 122:463–467
12. Sano D, Yamamoto Y, Samejima T, Seita Y, Inomata T, Ito J et al (2009) A combined treatment with ethanol and 6-dimethylaminopurine is effective for the activation and further embryonic development of oocytes from Sprague-Dawley and Wistar rats. Zygote 17:29–36
13. Otsuki J, Nagai Y, Chiba K (2007) Peroxidation of mineral oil used in droplet culture is detrimental to fertilization and embryo development. Fertil Steril 88:741–743
14. Jiang J-Y, Tsang BK (2004) Optimal conditions for successful in vitro fertilization and subsequent embryonic development in Sprague-Dawley rats. Biol Reprod 71: 1974–1979
15. Nakatsukasa E, Kashiwazaki N, Takizawa A, Shino M, Kitada K, Serikawa T et al (2003) Cryopreservation of spermatozoa from closed colonies, and inbred, spontaneous mutant, and transgenic strains of rats. Comp Med 53:639–641

BRAIN RESEARCH 1309 (2010) 104–109

available at www.sciencedirect.com

ScienceDirect

www.elsevier.com/locate/brainres

BRAIN RESEARCH

Research Report

Effects of levetiracetam on hippocampal kindling in Noda epileptic rats

Yuji Ishimaru[a,*], *Shigeru Chiba*[a], *Tadao Serikawa*[b], *Masashi Sasa*[c], *Hiroko Inaba*[a], *Yoshiyuki Tamura*[a], *Takahiro Ishimoto*[a], *Hideki Takasaki*[a], *Kazutaka Sakamoto*[a], *Kazuhide Yamaguchi*[a]

[a]*Department of Psychiatry and Neurology, Asahikawa Medical College, Midorigaoka higashi 2-1-1-1, Asahikawa, 078-8510, Japan*
[b]*Institute of Laboratory Animals, Kyoto University, Kyoto, Japan*
[c]*Nagisa Hospital, Osaka, Japan*

ARTICLE INFO

Article history:
Accepted 22 October 2009
Available online 29 October 2009

Keywords:
Epilepsy
Antiepileptic drug
Brainstem
Secondary generalization

ABSTRACT

In order to clarify the seizure susceptibility of Noda epileptic rat (NER) and the antiepileptic effects of levetiracetam (LEV), we performed electrical hippocampal kindling in NERs compared with Wistar rats (experiment 1), and hippocampal kindling in NERs with LEV administration (experiment 2). In experiment 1, electrical stimulation was administered to the right dorsal hippocampus of NERs and Wistar rats once per day. In experiment 2, NERs were randomly assigned to group L (LEV administration) and C (saline administration). Following daily administration of LEV (240 mg/kg, i.p.) to group L and saline to group C, hippocampal kindling was performed from the 5th day of consecutive LEV or saline administration. As a result of experiment 1, all NERs exhibited stage 5 (falling) or stage 6 seizure (running/jumping, subsequent seizure) from the first electrical stimulation. In experiment 2, LEV suppressed development of hippocampal kindling, increased the afterdischarge threshold of the hippocampus and inhibited stage 6 seizures in NER. Although LEV prolonged the afterdischarge duration at the first stage 5 seizure significantly, there was a tendency to prolong the latency to generalization by LEV. These findings indicate that NER is susceptible not only to limbic seizures but also to brainstem seizures. Furthermore, LEV may have inhibitory effects not only on the hippocampus but also on other neuronal pathways to secondary generalization in this rat model.

1. Introduction

Levetiracetam (LEV) is a new antiepileptic drug used widely and clinically, which is indicated as adjunctive therapy in the treatment of partial onset seizures with partial epilepsy with or without secondary generalization, myoclonic seizures with juvenile myoclonic epilepsy and primary generalized tonic–clonic seizures with idiopathic generalized epilepsy. It has no serious side effects (French et al., 2001) and no interaction with other antiepileptic drugs (Patsalos, 2000).

In experimental animal models, LEV has no anticonvulsant activity in the acute maximal electroshock seizure test or the maximal pentylenetetrazol seizure test in mice, both of which have been used as methods for screening for anticonvulsive

* *Corresponding author.* Fax: +81 166 68 2479.
E-mail address: ishimaru@asahikawa-med.ac.jp (Y. Ishimaru).

0006-8993/$ – see front matter © 2009 Elsevier B.V. All rights reserved.
doi:10.1016/j.brainres.2009.10.056

effects of antiepileptic drugs (Klitgaard et al., 1998). However, LEV has potent protections against generalized epileptic seizures in corneal electroshock and pentylenetetrazol-kindled seizures in mice (Klitgaard et al., 1998). LEV also suppresses development of amygdala-kindling process in rats (Löscher et al., 1998; Stratton et al., 2003). Furthermore, in spontaneously epileptic rats (SER), the antiepileptic effects against tonic convulsions and absence-like seizures are observed not only during the LEV-administration period but also several days after the final administration of LEV (Ji-qun et al., 2005).

At the neuronal level, LEV has no effect on neuronal voltage-activated Na^+ or T-type Ca^{2+} currents (Zona et al., 2001) and no direct actions on γ-aminobutyric acid (GABA) or glutamate receptors (Sills et al., 1997; Tong & Patsalos, 2001; Margineanu & Klitgaard, 2003), the mechanisms common for most antiepileptic drugs currently available. On the other hand, LEV moderately inhibits both N-type Ca^{2+} channels (Niespodziany et al., 2001) and the delayed rectifier K^+ current (Madeja et al., 2003), and opposes the inhibitory action of zinc on GABA and glycine-gated current (Rigo et al., 2002). Furthermore, LEV has a specific binding site identified as the synaptic vesicle protein 2A (SV2A), which supposedly plays a role in the exocytosis of neurotransmitters (Lynch et al., 2004). In rat hippocampal slices, LEV reduces both the amplitude and the number of population spikes, produced by a "high K^+-low Ca^{2+}" perfusion fluid in the CA3 area, more intensively than valproate, clonazepam and carbamazepine (Margineanu and Klitgaard, 2000).

Noda epileptic rat (NER) is a natural mutant rat found in a Wistar colony (Noda et al., 1998). NER exhibits spontaneous generalized tonic–clonic seizures after 2–4 months of age (approximately once per 30 h at the ages of between 14 and 27 weeks), which persists indefinitely, and has no organic brain lesions (Noda et al., 1998). Therefore, NER may serve as a prominent animal model for generalized tonic–clonic seizures in humans. NER also exhibits audiogenic seizures (AGS) if weekly sound stimulations are received repeatedly from 3 to 9 weeks of age (Iida et al., 1998). This AGS is strongly inhibited by carbamazepine, phenobarbital or valproate (Sasa et al., 1997). The hippocampus may play a role in epileptogenicity in NER because hippocampal CA3 neurons have abnormal firings by a single electrical stimulus only in youth (seven of 14 hippocampal CA3 neurons at 4–6 weeks of age; three of nine CA3 neurons at 10–15 weeks of age; none of 10 neurons more than 20 weeks of age) (Hanaya et al., 2002).

The advantage of the experiments using genetic animal models of epilepsy is that they simulate the clinical situation more closely than any other experimental epilepsy (Löscher, 1984). To our knowledge, there is no study of the effects of LEV on seizures of natural epilepsy mutant rats except GAERS (Klitgaard et al., 1998, Dedeurwaerdere et al., 2005). In order to clarify the seizure susceptibility of NER and the antiepileptic effects of LEV in NER, we had evaluated (1) spontaneous generalized tonic–clonic seizures and (2) hippocampal kindling establishments in NER (compared with Wistar rat).

We had also evaluated the anticonvulsant effects of LEV on the behavioral and electroencephalographical seizures.

Table 1 – Development of hippocampal kindling in NERs and Wistar rats in experiment 1.

	Number of stimulations required to reach stage 5	Kindling completion	Number of rats with stage 6
NER, $n=5$	1.0* (1–1)	3.0* (3–3)	4/5†
Wistar rat, $n=5$	16.6 (10–28)	20.6 (15–30)	0/5

Values are: means (numbers in parentheses; range). *$p=0.005$ (by Mann–Whitney U test) and †$p=0.048$ (by Fisher's exact test) as compared with corresponding control values.

2. Results

2.1. *Experiment 1*

The number of stimulations required to reach first stage 5 or stage 6 seizure in the NER group was significantly smaller than that of the control group ($p=0.005$) (Table 1). Similarly, the number of stimulations required to produce completion of kindling in the NER group was significantly smaller than that of the control group ($p=0.005$). The number of NERs that exhibited stage 6 seizures was significantly larger than that of Wistar rats ($p=0.048$). There were no significant differences between the NER and control groups in the afterdischarge (AD) threshold (ADT) and in the AD duration (ADD) (Table 2). Fig. 1 shows representative EEGs of the NER group. Running and generalized convulsions, which are not generally shown in hippocampal kindling in normal Wistar rats, were exhibited in some NERs (Fig. 1A). Furthermore, this NER also exhibited subsequent seizure (generalized convulsions) after kindled seizure (Fig. 1B).

2.2. *Experiment 2*

The number of stimulations required to reach first stage 5 or stage 6 seizure in group L was significantly larger than that of group C ($p<0.001$) (Table 3). Similarly, the number of stimulations required to produce completion of kindling in group L was significantly larger than that of group C ($p<0.001$). Moreover, the number of NERs in group L that exhibited stage 6 seizures was significantly smaller than that of group C ($p=0.033$). Fig. 2 shows representative EEGs of each group. Stage 6 seizures were exhibited in some NERs of group C (Fig. 2A), but not in those of group L (Fig. 2B).

The ADT at the first seizure in group L was significantly higher than that of group C ($p=0.021$) (Table 4). The ADD at the

Table 2 – ADT and ADD in NERs and Wistar rats in experiment 1.

	ADT [μA]	ADD [sec]
NER, $n=5$	50.0 (25–100)	94.4 (90–137)
Wistar rat, $n=5$	30.0 (25–50)	112.8 (97–154)

Values are: means (numbers in parentheses; range). ADT, afterdischarge threshold at the first electrical stimulation; ADD, afterdischarge duration at the first stage 5 seizure.

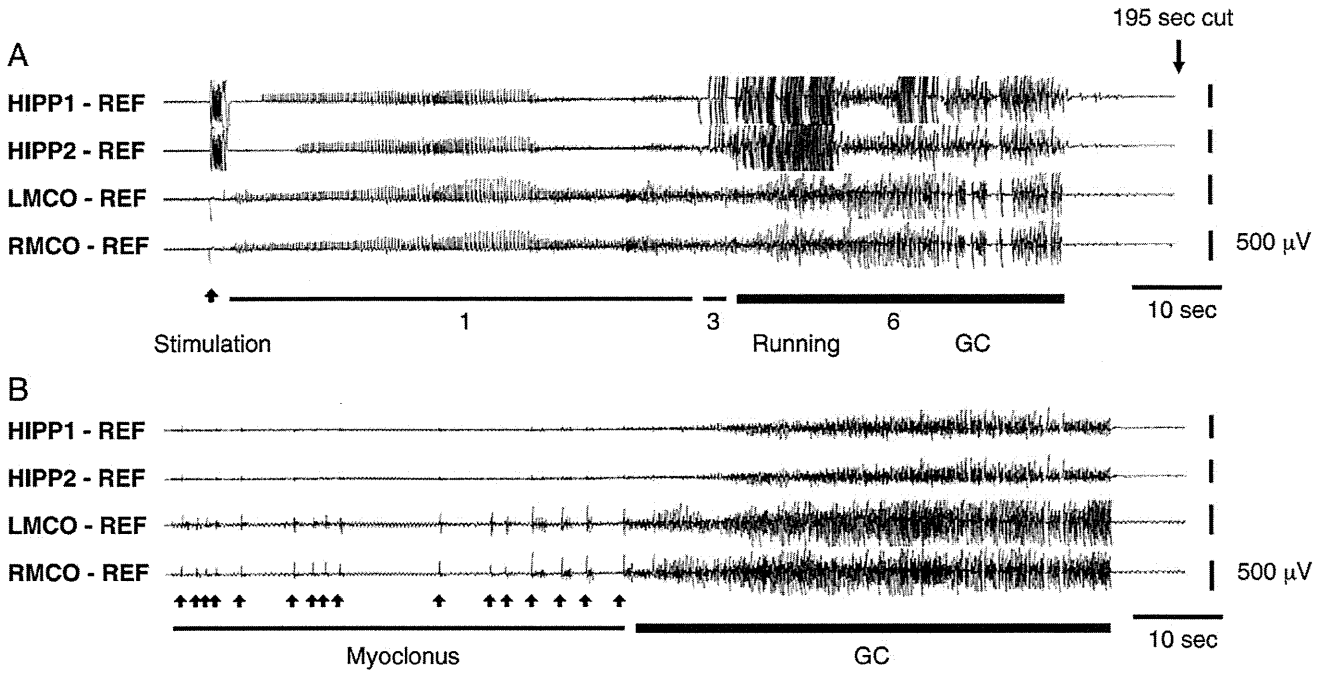

Fig. 1 – EEGs of kindled seizure and subsequent seizure after kindled seizure in the same NER in experiment 1. (A) Stage 6 seizure. (B) Subsequent seizure after 195 s of kindled seizure. Each number corresponds to the individual stage of seizure as mentioned in methods. HIPP, hippocampus; LMCO, left motor cortex; RMCO, right motor cortex; REF, reference; GC, generalized convulsion.

first stage 5 seizure in group L was significantly longer than that of group C ($p=0.010$). The time required for the seizure to be generalized at the first stage 5 seizure in group L tended to be longer than that of group C ($p=0.082$), but no significant differences were observed between them.

3. Discussion

We had confirmed that NER exhibit spontaneous generalized tonic–clonic seizures as previously described (Noda et al., 1998). NER is a natural mutant rat found in a Wistar colony and, thus, may serve a prominent animal model for generalized tonic–clonic seizures in humans. The limitation of using NER is also noted, and the infrequent occurrence seizure is not practical for the systematic pharmacological experiments to evaluate anticonvulsants. We therefore also evaluated if NER is more susceptible for the establishments of the hippocampal kindling compared to wildtype Wistar rats.

Table 3 – Development of hippocampal kindling in group L and C in experiment 2.

	Number of stimulations required to reach stage 5	Kindling completion	Number of rats with stage 6
Group L, $n=10$	2.8* (1–5)	5.5* (3–12)	0/10†
Group C, $n=10$	1.0 (1–1)	3.0 (3–3)	5/10

Values are: means (numbers in parentheses; range). *$p<0.001$ (by Mann–Whitney U test) and †$p=0.033$ (by Fisher's exact test) as compared with corresponding control values.

In experiment 1, group NER showed a marked facilitation of hippocampal kindling. All NERs, but not wildtype Wistar rats, exhibited stage 5 or stage 6 seizure (running/jumping, subsequent seizure) consecutively during the initial 3 electrical stimulation sessions and, thus, established the hippocampal kindling rapidly. Since the competition of the kindling was only recorded at 3.0 days in not wildtype Wistar rats (average of the 5 rats), the NER is susceptible to the hippocampal kindling, and the hippocampal kindling model of NER may thus be useful for pharmacological experiments to predict efficacy of candidate antiepileptic drugs for human conditions.

In addition, since NER exhibit several behavioral seizure activities, such as AGS and the tonic extension phase, the model may also be useful to understand basic mechanisms of generations of seizure activities. In genetically epilepsy-prone rats, wild running behavior during AGS is thought to be induced by the neuron's activity of the deep layers of superior colliculus (Faingold and Randall, 1999), and the tonic extension phase seems to be driven by the pontine reticular formation (Faingold and Randall, 1995). Therefore, these manifestations are thought to be driven by the brainstem, and NER may have enhanced susceptibilities to neuroplastic changes in the brainstem. Subsequent amygdala kindling after the interpeduncular nucleus (IPN) kindling in rats shows more rapid kindling and tonic seizure not observed in rats undergoing amygdala kindling without previous IPN kindling (Chiba and Wada, 1995). This phenomenon may resemble the findings of the present study. In our previous study, NER also exhibited a noticeable facilitation of amygdala kindling

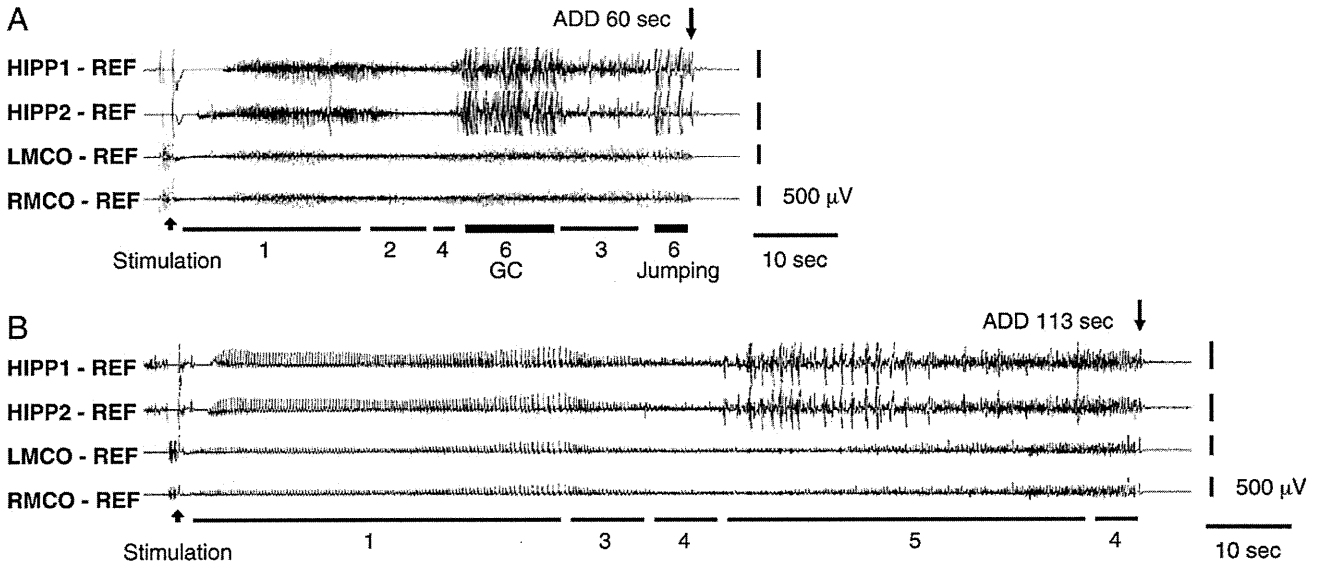

Fig. 2 – EEGs of each group in experiment 2. (A) Stage 6 seizure in group C. (B) Stage 5 seizure in group L. Each number corresponds to the individual stage of seizure as mentioned in methods. HIPP, hippocampus; LMCO, left motor cortex; RMCO, right motor cortex; REF, reference; GC, generalized convulsion; ADD, afterdischarge duration.

accompanied with stage 6 seizures (Omori et al., 2001). These findings suggest that NER is susceptible to not only limbic seizures, but also brainstem seizures.

In experiment 2, LEV suppressed development of hippocampal kindling, increased the ADT of the hippocampus and inhibited stage 6 seizures in NER. GTCS in NER has been thought to be suppressed mainly by blocking of Na^+ channels because AGS in NER is strongly inhibited by carbamazepine, phenobarbital and valproate (Sasa et al., 1997). Furthermore, the candidate causative gene for spontaneous tonic–clonoic seizure codes for Na^+ channels in NER (Maihara et al., 2000). However, LEV has no inhibitory effects on Na^+ channels (Zona et al., 2001). Additionally, LEV has moderate inhibitory effects of N-type Ca^{2+} channels (Niespodziany et al., 2001), although the abnormal excitability of NER hippocampal CA3 neurons (Hanaya et al., 2002) is not inhibited by the N-type Ca^{2+} channel antagonist, omega-conotoxin GVIA (Kiura et al., 2003). Therefore, the mechanism of the inhibitory effects of LEV on seizures in NER is unknown at this moment. Since LEV has a specific binding site identified as the SV2A, there is a possibility that the seizure of NER is inhibited via SV2A. Although the mechanism of SV2A for exhibiting anticonvulsant activity is not fully understood (Rogawski, 2006), there is a correlation between binding affinity to SV2A and potency in suppressing seizures in sound-susceptible mice (Lynch et al., 2004).

Table 4 – ADT, ADD and Latency to GS in group L and C in experiment 2.

	ADT [μA]	ADD [s]	Latency to GS [s]
Group L, $n=10$	120.0* (25–400)	141.8† (109–191)	66.7‡ (23–106)
Group C, $n=10$	40.0 (25–100)	109.5 (82–137)	51.5 (26–74)

Values are: means (numbers in parentheses; range). *$p=0.021$, †$p=0.010$ and ‡$p=0.082$ (by Mann–Whitney U test) as compared with corresponding control values. ADT, afterdischarge threshold at the first electrical stimulation; ADD, afterdischarge duration at the first stage 5 seizure; GS, generalized seizure.

LEV may have inhibitory effects on the electrically produced abnormal firing in the hippocampus because of the current finding of increase of the ADT at the hippocampus by LEV administration. It has also been reported that LEV reduces both the amplitude and the number of population spikes in rat hippocampal slices (Margineanu and Klitgaard, 2000). However, if the SV2 binding property is involved in the anticonvulsant activity of LEV, effects on other brain sites, such as the amygdala, may also be involved since SV2A is expressed ubiquitously throughout the brain (Bajjalieh et al., 1994; Tong and Patsalos, 2001).

Some experiments show a correlation between the severity of kindled seizure and the ADD (Löscher et al., 1998; Stratton et al., 2003). In the present study, however, ADD at the first stage 5 or stage 6 seizure in group L was significantly longer than that of group C, though the severity of seizures in group L was lower. On the other hand, there was a tendency to prolong the latency to generalization by LEV (until showing bilateral forelimb clonus) at the first stage 5 seizure in group L ($p=0.082$). It is reported that LEV, as well as phenobarbital or clonazepam, reduces the severity of pilocarpine-induced and kainic acid-induced generalized seizures in mice or rats (Klitgaard et al., 1998), unlike the other antiepileptic drugs (carbamazepine or phenytoin) (Turski et al., 1987; Klitgaard et al., 1998). It has also been reported that the earliest electrographic responses to i.p. administered pilocarpine or kainic acid appear in the hippocampal area (Turski et al., 1983; Nadler, 1981), and after that, generalized seizure is shown. Therefore, LEV may have inhibitory effects on not only the hippocampus but also the neuronal pathway to generalization. Furthermore, Tilz et al. (2006) reported that adult patients with focal epilepsies under LEV treatment showed a prolonged

latency of the contralateral seizure pattern propagation in EEG, compared with under placebo. As above, LEV has potent inhibitory effects of secondary generalization.

The hippocampus may play a role in epileptogenicity in NER, because hippocampal CA3 neurons have abnormal firings only in youth (Hanaya et al., 2002). As mentioned, LEV may possess a function of suppressing the abnormal discharges in the hippocampus. Therefore, it may be possible to inhibit the development of epileptogenicity in NER by suppressing the abnormal firing in the hippocampus through use of LEV before they display any seizures. In this regard, it is reported that the incidence of tonic seizures or absence-like seizures decreases in SER if LEV is administered before they show tonic seizures (Yan et al., 2005). These results suggest a possibility that LEV inhibits the development of epileptogenicity in NER and some forms of epilepsy of NER would be preventable by LEV. As a result, further experiments along with this line are warranted.

4. Experimental procedures

4.1. *Experiment 1*

Adult male NERs ($n=5$) and Wistar rats ($n=5$) (4-6 months of age, 350-560 g) were used. Under pentobarbital anesthesia, bipolar electrodes, made of twisted wire, 200 μm in diameter, were stereotaxically (Paxinos and Watson, 1998) implanted into the right dorsal hippocampus (3.3 mm posterior and 2.0 mm lateral from bregma, 3.6 mm ventral to the skull). Three surface electrodes (stainless steel screws) were driven into the skull: two for recording from the bilateral motor cortex, and the other to be placed over the cerebellar cortex as a reference electrode.

We first evaluated the spontaneous generalized tonic–clonic seizures in NERs. Although we had confirmed that these animals had occasional behavioral seizures accompanied with anomaly EEG (Noda et al., 1998), they were not severely affected and less than one attack, lasting no more than 2 minutes, was observed per day. This made evaluation of the effect of anticonvulsants systematically in these the spontaneous attacks impractical. We therefore evaluated if these rats were more susceptible to establish the hippocampal kindling and if these seizures can be used for the pharmacological evaluation of an anticonvulsant, LEV.

For the hippocampal kindling experiments, electrical stimulation (60 Hz biphasic square pulses of a 1-s duration) which induced afterdischarge (AD), was administered to the hippocampus of NER and control groups once per day starting from 1 week after the implantation. The AD threshold (ADT) of the hippocampus was determined by 1-s stimulation beginning at 25 μA (60 Hz biphasic square pulses) with subsequent increases made in 25 μA steps at 10-min intervals until AD was induced.

The kindled seizures were classified by a modification of Racine (1972), as follows: stage 1, behavioral arrest or mouth/facial movements; stage 2, head nodding; stage 3, forelimb clonus; stage 4, rearing; stage 5, falling; stage 6, falling accompanied by jumping/running and/or subsequent seizure. Completion of kindling was recorded when stage 5 or stage 6 seizures were observed for 3 consecutive experimental days. Electrical stimulation was continued until obtaining completion of kindling, but discontinued once kindling was established.

Data were recorded on the digital EEG with video recording for 20 min after electrical stimulation. Statistics were compared using Mann–Whitney U test or Fisher's exact test, and $p<0.05$ (two-tailed) was considered a significant difference.

4.2. *Experiment 2*

Twenty adult male NERs (4–6 months of age, 350-560 g) were used. They were randomly assigned to group L (LEV administration, $n=10$) and C (saline administration, $n=10$). One week after implantation of electrodes, daily administration of LEV (240 mg/kg, i.p.), dissolved in saline (2.4 ml/kg), to group L and saline (2.4 ml/kg) to group C was started. Hippocampal kindling was performed by electrical stimulation, which induced AD from the 5th day of consecutive LEV or saline administration. The electrical stimulations were provided after 30 min of each administration, and the administrations were continued until completion of kindling.

The dose of 240 mg/kg, i.p. was used since other researchers used a similar dose range in rats (van Vliet et al., 2008; Glien et al., 2002). The dose was relatively high for common clinical use (a clinical dose of 500–5000 mg/day is 8.3–83.3 mg/kg in 60 kg body weight), but the plasma elimination half life in rats is much shorter, 2 to 3 h compared to 6 to 8 h in humans. It was also reported that the dose 240 mg/kg, i.p. of LEV doesn't cause behavioral alterations in rats (Klitgaard et al., 1998).

Hippocampal kindling was started at 5th day of consecutive LEV or saline administration since chronic effects of LEV were intended to be detected.

The method of implantation of electrodes, determination of ADT, classification of seizures, definition of completion of kindling, data recording and statistics were the same as experiment 1.

All experiments were performed under the guidelines for animal experiments stipulated at Asahikawa Medical College.

Acknowledgments

The authors wish to thank Prof. Yoshikatsu Mochizuki for statistical analyses. This study was supported by UCB Pharma.

REFERENCES

Bajjalieh, S.M., Frantz, G.D., Weimann, J.M., McConnell, S.K., Scheller, R.H., 1994. Differential expression of synaptic vesicle protein 2 (SV2) isoforms. J. Neurosci. 14, 5223–5235.

Chiba, S., Wada, J.A., 1995. Kindling of the interpeduncular nucleus and its influence on subsequent amygdala kindling in rats. Epilepsia 36, 410–415.

Dedeurwaerdere, S., Boon, P., De Smedt, T., Claeys, P., Raedt, R., Bosman, T., Van Hese, P., Van Maele, G., Vonck, K., 2005. Chronic levetiracetam treatment early in life decreases epileptiform events in young GAERS, but does not prevent the expression of spike and wave discharges during adulthood. Seizure 14, 403–411.

Faingold, C.L., Randall, M.E., 1995. Pontine reticular formation neurons exhibit a premature and precipitous increase in acoustic responses prior to audiogenic seizures in genetically epilepsy-prone rats. Brain Res. 704, 218–226.

Faingold, C.L., Randall, M.E., 1999. Neurons in the deep layers of superior colliculus play a critical role in the neuronal network for audiogenic seizures: mechanisms for production of wild running behavior. Brain Res. 815, 250–258.

French, J., Edrich, P., Cramer, J.A., 2001. A systematic review of the safety profile of levetiracetam: a new antiepileptic drug. Epilepsy Res. 47, 77–90.

Glien, M., Brandt, C., Potschka, H., Löscher, W., 2002. Effects of the novel antiepileptic drug levetiracetam on spontaneous recurrent seizures in the rat pilocarpine model of temporal lobe epilepsy. Epilepsia 43, 350–357.

Hanaya, R., Sasa, M., Kiura, Y., Ishihara, K., Serikawa, T., Kurisu, K., 2002. Epileptiform burst discharges in hippocampal CA3 neurons of young but not mature Noda epileptic rats (NER). Brain Res. 950, 317–320.

Iida, K., Sasa, M., Serikawa, T., Noda, A., Ishihara, K., Akimitsu, T., Hanaya, R., Arita, K., Kurisu, K., 1998. Induction of convulsive seizures by acoustic priming in a new genetically defined model of epilepsy (Noda epileptic rat: NER). Epilepsy Res. 30, 115–126.

Ji-qun, C., Ishihara, K., Nagayama, T., Serikawa, T., Sasa, M., 2005. Long-lasting antiepileptic effects of levetiracetam against epileptic seizures in the spontaneously epileptic rat (SER): differentiation of levetiracetam from conventional antiepileptic drugs. Epilepsia 46, 1362–1370.

Kiura, Y., Hanaya, R., Serikawa, T., Kurisu, K., Sakai, N., Sasa, M., 2003. Involvement of Ca^{2+} channels in abnormal excitability of hippocampal CA3 pyramidal cells in noda epileptic rats. J. Pharmacol. Sci. 91, 137–144.

Klitgaard, H., Matagne, A., Gobert, J., Wölfert, E., 1998. Evidence for a unique profile of levetiracetam in rodent models of seizures and epilepsy. Eur. J. Pharmacol. 353, 191–206.

Löscher, W., 1984. Genetic animal models of epilepsy as a unique resource for the evaluation of anticonvulsant drugs. A review. Methods Find. Exp. Clin. Pharmacol. 6, 531–547.

Löscher, W., H?nack, D., Rundfeldt, C., 1998. Antiepileptogenic effects of the novel anticonvulsant levetiracetam (ucb L059) in the kindling model of temporal lobe epilepsy. J. Pharmacol. Exp. Ther. 284, 474–479.

Lynch, B.A., Lambeng, N., Nocka, K., Kensel-Hammes, P., Bajjalieh, S.M., Matagne, A., Fuks, B., 2004. The synaptic vesicle protein SV2A is the binding site for the antiepileptic drug levetiracetam. Proc. Natl. Acad. Sci. U. S. A. 101, 9861–9866.

Madeja, M., Margineanu, D.G., Gorji, A., Siep, E., Boerrigter, P., Klitgaard, H., Speckmann, E.J., 2003. Reduction of voltage-operated potassium currents by levetiracetam: a novel antiepileptic mechanism of action Neuropharmacology 45, 661–671.

Maihara, T., Noda, A., Yamazoe, H., Voigt, B., Kitada, K., Serikawa, T., 2000. Chromosomal mapping of genes for epilepsy in NER: a rat strain with tonic–clonic seizures. Epilepsia 41, 941–949.

Margineanu, D.G., Klitgaard, H., 2000. Inhibition of neuronal hypersynchrony *in vitro* differentiates levetiracetam from classical antiepileptic drugs. Pharmacol. Res. 42, 281–285.

Margineanu, D.G., Klitgaard, H., 2003. Levetiracetam has no significant gamma-aminobutyric acid-related effect on paired-pulse interaction in the dentate gyrus of rats. Eur. J. Pharmacol. 466, 255–261.

Nadler, J.V., 1981. Kainic acid as a tool for the study of temporal lobe epilepsy. Life Sci. 29, 2031–2042.

Niespodziany, I., Klitgaard, H., Margineanu, D.G., 2001. Levetiracetam inhibits the high-voltage-activated Ca^{2+} current in pyramidal neurones of rat hippocampal slices. Neurosci. Lett. 306, 5–8.

Noda, A., Hashizume, R., Maihara, T., Tomizawa, Y., Ito, Y., Inoue, M., Kobayashi, K., Asano, Y., Sasa, M., Serikawa, T., 1998. NER rat strain: a new type of genetic model in epilepsy research. Epilepsia 39, 99–107.

Omori, N., Tabata, K., Ishimaru, Y., Ishimoto, T., Tamura, Y., Mutoh, F., Chiba, S., Ohta, S., Kiura, Y., Akimitsu, T., Hanaya, R., Kurisu, K., Sasa, M., Serikawa, T., 2001. Amygdala kindling in Noda epileptic rat (NER). (in Japanese). Jpn. J. Clin. Neurophysiol. 29 (2), 200.

Patsalos, P.N., 2000. Pharmacokinetic profile of levetiracetam: toward ideal characteristics. Pharmacol. Ther. 85, 77–85.

Paxinos, G., Watson, C., 1998. The Rat Brain in Stereotaxic Coordinates, Fourth Edition. Academic Press, Sydney.

Racine, R.J., 1972. Modification of seizure activity by electrical stimulation. II. Motor seizure. Electroencephalogr. Clin. Neurophysiol. 32, 281–294.

Rigo, J.M., Hans, G., Nguyen, L., Rocher, V., Belachew, S., Malgrange, B., Leprince, P., Moonen, G., Selak, I., Matagne, A., Klitgaard, H., 2002. The anti-epileptic drug levetiracetam reverses the inhibition by negative allosteric modulators of neuronal GABA- and glycine-gated currents. Br. J. Pharmacol. 136, 659–672.

Rogawski, M.A., 2006. Diverse mechanisms of antiepileptic drugs in the development pipeline. Epilepsy Res. 69, 273–294.

Sasa, M., Hanaya, R., Iida, K., Akimitsu, T., Kurisu, K., Noda, A., Serikawa, T., 1997. A novel epilepsy animal model (NER). Nihon Shinkei Seishin Yakurigaku Zasshi 17, 35–38.

Sills, G.J., Leach, J.P., Fraser, C.M., Forrest, G., Patsalos, P.N., Brodie, M.J., 1997. Neurochemical studies with the novel anticonvulsant levetiracetam in mouse brain. Eur. J. Pharmacol. 325, 35–40.

Stratton, S.C., Large, C.H., Cox, B., Davies, G., Hagan, R.M., 2003. Effects of lamotrigine and levetiracetam on seizure development in a rat amygdala kindling model. Epilepsy Res. 53, 95–106.

Tilz, C., Stefan, H., Hopfengaertner, R., Kerling, F., Genow, A., Wang-Tilz, Y., 2006. Influence of levetiracetame on ictal and postictal EEG in patients with partial seizures. Eur. J. Neurol. 13, 1352–1358.

Tong, X., Patsalos, P.N., 2001. A microdialysis study of the novel antiepileptic drug levetiracetam: extracellular pharmacokinetics and effect on taurine in rat brain. Br. J. Pharmacol. 133, 867–874.

Turski, W.A., Cavalheiro, E.A., Schwarz, M., Czuczwar, S.J., Kleinrok, Z., Turski, L., 1983. Limbic seizures produced by pilocarpine in rats: behavioural, electroencephalographic and neuropathological study. Behav. Brain Res. 9, 315–335.

Turski, W.A., Cavalheiro, E.A., Coimbra, C., Coimbra, C., Ikonomidou-Turski, C., Turski, L., 1987. Only certain antiepileptic drugs prevent seizures induced by pilocarpine. Brain Res. 434, 281–305.

van Vliet, E.A., van Schaik, R., Edelbroek, P.M., da Silva, F.H., Wadman, W.J., Gorter, J.A., 2008. Development of tolerance to levetiracetam in rats with chronic epilepsy. Epilepsia 49, 1151–1159.

Yan, H.D., Ji-qun, C., Ishihara, K., Nagayama, T., Serikawa, T., Sasa, M., 2005. Separation of antiepileptogenic and antiseizure effects of levetiracetam in the spontaneously epileptic rat (SER). Epilepsia 46, 1170–1177.

Zona, C., Niespodziany, I., Marchetti, C., Klitgaard, H., Bernardi, G., Margineanu, D.G., 2001. Levetiracetam does not modulate neuronal voltage-gated Na^+ and T-type Ca^{2+} currents. Seizure 10, 279–286.

OPEN ACCESS Freely available online

PLoS one

Induction and Enhancement of Cardiac Cell Differentiation from Mouse and Human Induced Pluripotent Stem Cells with Cyclosporin-A

Masataka Fujiwara[1,2], Peishi Yan[1,3¤], Tomomi G. Otsuji[4,5], Genta Narazaki[1,6], Hideki Uosaki[1,6], Hiroyuki Fukushima[1,6], Koichiro Kuwahara[2], Masaki Harada[2], Hiroyuki Matsuda[7], Satoshi Matsuoka[7], Keisuke Okita[8], Kazutoshi Takahashi[8], Masato Nakagawa[8], Tadashi Ikeda[3], Ryuzo Sakata[3], Christine L. Mummery[9], Norio Nakatsuji[10,11], Shinya Yamanaka[8,12], Kazuwa Nakao[2], Jun K. Yamashita[1,6]*

1 Laboratory of Stem Cell Differentiation, Stem Cell Research Center, Institute for Frontier Medical Sciences, Kyoto University, Kyoto, Japan, **2** Department of Medicine and Clinical Science, Kyoto University Graduate School of Medicine, Kyoto, Japan, **3** Department of Cardiovascular Surgery, Kyoto University Graduate School of Medicine, Kyoto, Japan, **4** Stem Cell and Drug Discovery Institute, Kyoto Research Park, Kyoto, Japan, **5** Laboratory of Embryonic Stem Cell Research, Stem Cell Research Center, Institute for Frontier Medical Sciences, Kyoto University, Kyoto, Japan, **6** Department of Cell Growth and Differentiation, Center for iPS Cell Research and Application (CiRA), Kyoto University, Kyoto, Japan, **7** Department of Physiology and Biophysics, Kyoto University Graduate School of Medicine, Kyoto, Japan, **8** Department of Reprogramming Science, Center for iPS Cell Research and Application (CiRA), Kyoto University, Kyoto, Japan, **9** Department of Anatomy and Embryology, Leiden University Medical Centre, Leiden, the Netherlands, **10** Department of Development and Differentiation, Institute for Frontier Medical Sciences, Kyoto University, Kyoto, Japan, **11** Institute for Integrated Cell-Material Sciences (iCeMS), Kyoto University, Kyoto, Japan, **12** Gladstone Institute of Cardiovascular Disease, San Francisco, California, United States of America

Abstract

Induced pluripotent stem cells (iPSCs) are novel stem cells derived from adult mouse and human tissues by reprogramming. Elucidation of mechanisms and exploration of efficient methods for their differentiation to functional cardiomyocytes are essential for developing cardiac cell models and future regenerative therapies. We previously established a novel mouse embryonic stem cell (ESC) and iPSC differentiation system in which cardiovascular cells can be systematically induced from Flk1$^+$ common progenitor cells, and identified highly cardiogenic progenitors as Flk1$^+$/CXCR4$^+$/VE-cadherin$^-$ (FCV) cells. We have also reported that cyclosporin-A (CSA) drastically increases FCV progenitor and cardiomyocyte induction from mouse ESCs. Here, we combined these technologies and extended them to mouse and human iPSCs. Co-culture of purified mouse iPSC-derived Flk1$^+$ cells with OP9 stroma cells induced cardiomyocyte differentiation whilst addition of CSA to Flk1$^+$ cells dramatically increased both cardiomyocyte and FCV progenitor cell differentiation. Spontaneously beating colonies were obtained from human iPSCs by co-culture with END-2 visceral endoderm-like cells. Appearance of beating colonies from human iPSCs was increased approximately 4.3 times by addition of CSA at mesoderm stage. CSA-expanded human iPSC-derived cardiomyocytes showed various cardiac marker expressions, synchronized calcium transients, cardiomyocyte-like action potentials, pharmacological reactions, and ultra-structural features as cardiomyocytes. These results provide a technological basis to obtain functional cardiomyocytes from iPSCs.

Citation: Fujiwara M, Yan P, Otsuji TG, Narazaki G, Uosaki H, et al. (2011) Induction and Enhancement of Cardiac Cell Differentiation from Mouse and Human Induced Pluripotent Stem Cells with Cyclosporin-A. PLoS ONE 6(2): e16734. doi:10.1371/journal.pone.0016734

Editor: Felipe Prosper, Clinica Universidad de Navarra, Spain

Received November 1, 2010; **Accepted** December 24, 2010; **Published** February 22, 2011

Funding: This study was supported by grants from the Ministry of Education, Science, Sports and Culture of Japan, the Ministry of Health, Labour and Welfare, the New Energy and Industrial Development Organization (NEDO) of Japan, the Project for Realization of Regenerative Medicine. The funders had no role in study design, data collection and analysis, decision to publish, or preparation of the manuscript.

Competing Interests: The authors have declared that no competing interests exist.

* E-mail: juny@frontier.kyoto-u.ac.jp

¤ Current address: Cardiovascular Department, Dalian Municipal Central Hospital, Dalian, China

Introduction

Induced pluripotent stem cells (iPSCs) are novel pluripotent stem cells generated from adult tissues by reprogramming originally with transduction of a few defined transcription factors, such as Oct4, Sox2, Klf4, and c-myc [1], [2]. Establishment of iPSC lines from adult human tissue is facilitating development of cell transplantation-based regenerative strategies and establishment of patient-derived cells as disease models. Efficient differentiation and dissecting the differentiation mechanisms of target cells would significantly contribute to elucidate the pathophysiology of diseases and provide a platform for developing new therapeutic strategies for specific diseases through such as drug discovery [3], [4].

Cardiomyocytes are a major target of regenerative medicine. Although cardiomyocyte differentiation has been reported from various progenitor and adult cell sources (e.g. bone marrow, cardiac biopsies, adipose tissue, umbilical cord, mesenchymal cells, etc), overall, the efficiencies of functional cardiomyocyte appearance have been still variable (<1–5%) [5]. Pluripotent cells, embryonic stem cells (ESCs) and iPSCs have thus emerged as among the most promising stem cell sources for inducing

functional cardiomyocytes in vitro. Several induction and purification methods have been reported, starting with either mouse or human ESCs. These include stem cell aggregation in suspension and growth as embryoid bodies (EBs), co-culture with stroma cells, serum-free culture in differentiation medium, or hypoxic culture [6], [7], [8], [9], [10], [11]. Overall, the efficiency of cardiomycyte differentiation in human ESCs [6] should be still lower than in mouse ESCs [8], [11]. In view of the similarities between iPSCs and ESCs, most cardiomyocyte induction methods from iPSCs are based on those tried and tested in ESCs. Several groups have thus reported cardiomyocyte formation from mouse iPSCs using either EBs or stroma cell co-culture [12], [13], [14]. Recently, several reports on cardiomyocyte induction from human iPSCs appeared with based on EB formation though the efficiencies are still varied [15], [16], [17], [18], [19]. Other new methods robust in human iPSCs remain to be explored and maybe of particular value for preparation of transplantation cell sources as well as dissecting the differentiation mechanisms and drug discovery.

Previously, we developed a novel ESC differentiation system that recapitulates early cardiovascular development in vivo [8], [20], [21]. Flk1 (also known as vascular endothelial growth factor (VEGF) receptor-2) is the earliest differentiation marker for endothelial cells (ECs) and blood cells, and is a marker of lateral plate mesoderm [21], [22]. We induced $Flk1^+$ cells from ESCs, purified them by fluorescence-activated cell sorting (FACS), and re-cultured the purified cells. We succeeded in inducing the major cardiovascular cell types from the common $Flk1^+$ progenitor cells: vascular ECs, mural cells (pericytes and vascular smooth muscle cells) [20] and cardiomyocytes [8]. When purified $Flk1^+$ cells were cultured on mouse bone marrow-derived stromal cells, OP9 cells, spontaneously beating cardiomyocytes as well as ECs can be induced within 3–4 days (Flk-d3-4) even from a single cell. We, thus, demonstrated that ESC-derived $Flk1^+$ cells serve as cardiovascular progenitors [8], [20], [23], which was further supported with following several mouse and human studies [9], [24], [25], [26]. We also identified a $Flk1^+$/$CXCR4^+$/vascular endothelial $cadherin^-$ (FCV) population as highly cardiogenic progenitor cells among the progeny of $Flk1^+$ mesoderm cells at the single cell level [8]. That is, in an intermediate stage of ESC differentiation between $Flk1^+$ mesoderm cells and cardiomyocytes (Flk-d2), purified FCV population could efficiently give rise to cardiomyocytes from a single cell. The cardiogenic potential of FCV cells was 15–20 times higher than that of other cell populations among the $Flk1^+$ cell progeny. We further confirmed FCV cells can differentiate into cardiomyocytes in vivo through cell transplantation experiments [11]. FCV cells, which are detected just 1–2 days before the cardiomyocyte appearance, are so far the nearest upstream cardiac progenitors to cardiomyocytes. This system proved amenable to induce various cardiovascular cells systematically from ESCs, explore novel differentiation methods, and dissect the differentiation processes [23], [27], [28]. Indeed, we recently succeeded in demonstrating that an immunosuppressant, cyclosporin-A (CSA) showed a novel potent effect specifically on $Flk1^+$ mesoderm cells to induce a dramatic increase in FCV cardiac progenitor cells and cardiomyocytes with the use of this ESC differentiation system [11]. That is, when CSA was added to $Flk1^+$ cells co-cultured on OP9 cells, appearance of FCV progenitor cells and cardiomyocytes were increased by 10–20 times.

Recently, we were able to systematically induce cardiovascular cells from mouse iPSCs in a way almost identical to that using mouse ESCs [12]. Here, we combined our technologies in ESCs and iPSCs and showed that FCV cardiac progenitors and cardiomyocytes were efficiently expanded from mouse iPSCs by CSA treatment. Moreover, we extended the CSA method to human iPSCs and showed that CSA also successfully worked in human iPSC differentiation and efficiently enhanced the appearance of spontaneously beating cells. Human iPSC-derived cardiomyocytes showed expected molecular, structural and functional features of human cardiomyocytes. We, thus, succeeded in inducing and enhancing cardiac cell differentiation from both mouse and human iPSCs.

Methods

Antibodies

Monoclonal antibodies (MoAbs) for murine E-cadhein (ECCD2), murine Flk1 (AVAS12) were prepared and labeled in our laboratory as described previously [8], [21], [29]. MoAb for cardiac troponin-T (cTnT) (1:2000) was purchased from Neo-Markers (Fremont, CA). For staining human ESCs and iPSCs, another MoAb for cTnT (1:100) was from Santa Cruz Biotechnology (Santa Cruz, CA). MoAbs for murine and human α-actinin (1:800) was from Sigma (St Louis, Mo). MoAb of phycoerithrin (PE)-conjugated AVAS12 was purchased from eBioscience (San Diego, CA). MoAbs for biotinylated-CXCR4 was purchased from BD Pharmingen (San Diego, CA). Anti-HCN4 (1:200) and anti-Cav3.2 (1:200) antibodies were from Chemicon (Temecula, CA). Anti-Kir2.1 (1:200) and anti-connexin 43 (1:200) antibodies were from Alomone (Israel) and Invitrogen (Carlsbad, CA), respectively.

Reagents

Cyclosporin-A (a gift from Novartis Pharma) was dissolved in Dimethyl sulfoxide (DMSO) (Nacalai Tesque, Kyoto Japan) at 30 mg/mL. Dilution of 1–3 μg/mL were made in differentiation medium at the time of use. PKH67 fluorescent dye was purchased from Sigma (St. Louis, MO).

Mouse iPSC culture

A germline-competent mouse iPSC line, 20D-17, carrying Nanog promoter-driven GFP/IRES/puromycin resistant gene (Nanog-iPS cells), was maintained as previously described [30]. Briefly, iPSCs were maintained in Dulbecco's Modified Eagle Medium (DMEM) containing 15% FCS, non-essential amino acids, 1 mmol/L sodium pyruvate, 5.5 mmol/L 2-mercaptoethanol, 50 units/mL penicillin and 50 mg/mL streptomycin on feeder layers of mitomycin-C-treated mouse embryonic fibroblast (MEF) cells carrying stably incorporated puromycin-resistance gene. OP9 stroma cells were maintained as described [21].

Induction of mouse cardiomyocyte differentiation

Induction of $Flk1^+$ cells and sorting for $Flk1^+$ cells were performed as previously described [8], [12], [20]. Briefly, mouse iPSCs were first plated on to gelatin-coated dishes and cultured for 30 min to eliminate attached feeder cells, then, non-adherent cells were collected and induced to differentiation. Mouse iPSCs were cultured at a density of $1–2.5\times10^3$ cells/cm^2 in differentiation medium (DM)(alpha minimum essential medium (GIBCO, Grand Island, NY) supplemented with 10% fetal calf serum) on type IV collagen-coated dishes (Biocoat, Beckton Dickinson) or mitomycin C-treated confluent OP9 cell sheets (MMC-OP9) for 96–108 h. Cells were collected and selected by FACS to purify $Flk1^+$ cells. $Flk1^+$ cells were then plated on to MMC-OP9 at a density of $1–10\times10^3$ cells/cm^2 and cultured in differentiation medium to induce cardiac differentiation. CSA (1–3 μg/mL) was added to $Flk1^+$ cells on OP9 cells. Medium was replaced every 2 days.

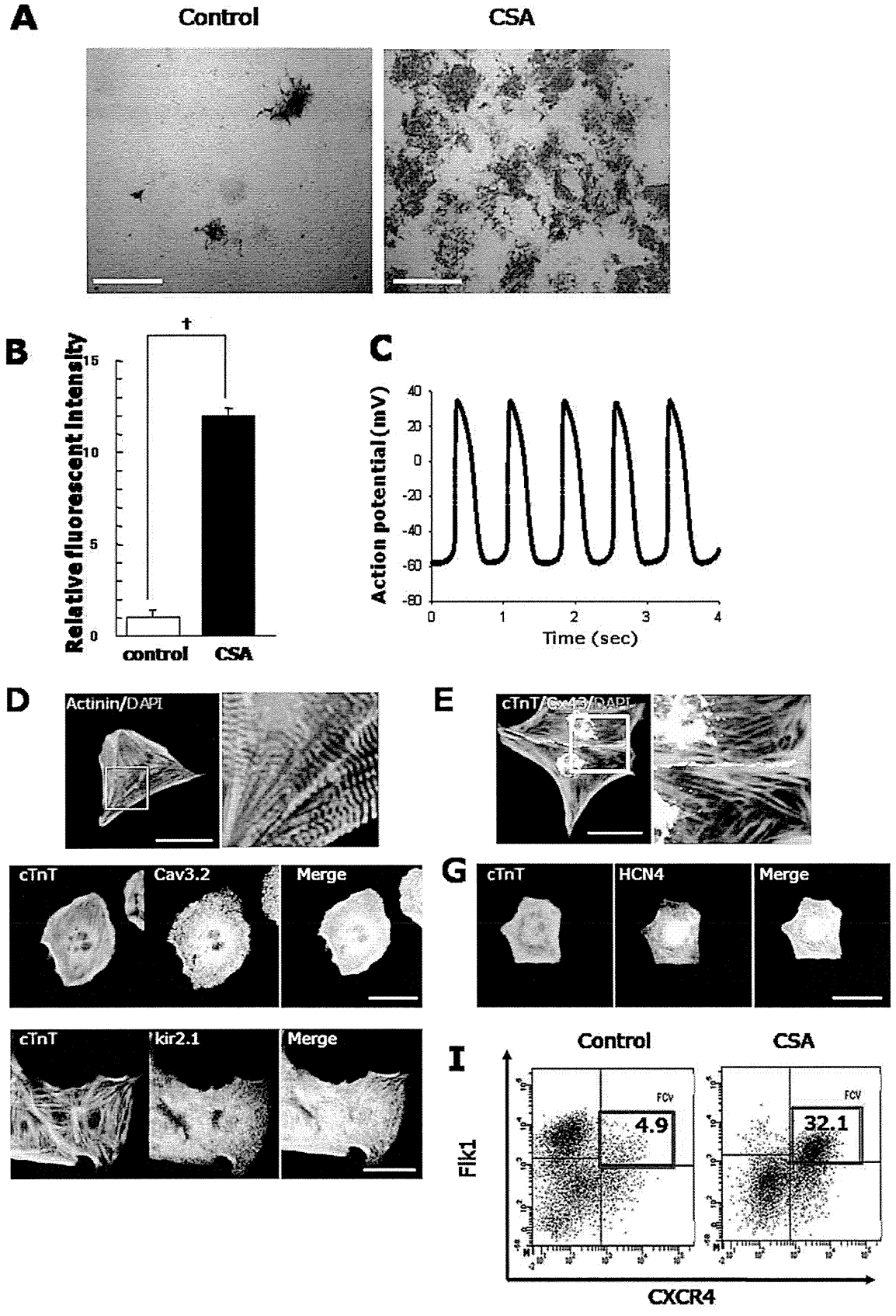

Figure 1. Cardiac cell expansion from mouse iPSC-derived Flk1$^+$ mesoderm by CSA. A. Gross appearance of cardiomyocyte induction by CSA. Six days after the Flk1$^+$ cell culture on OP9 cells (Flk-d6). cTnT staining (brown). Left panel: control. Right panel: CSA treatment. Scale bars = 400 μm. **B.** Quantitative evaluation of cardiomyocyte induction by fluorescent intensity of cTnT staining. Relative fluorescent intensity is

indicated (n = 4, †, $p<0.001$ vs control). **C.** Representative action potential of iPSC-derived spontaneously beating cardiomyocytes. **D.** Sarcomeric organization in TMRM-purified cardiomyocytes at Flk-d8. Immunostaining with anti-sarcomeric α-actinin antibody (red) and DAPI (blue). Right panel shows higher magnification of boxed area. Scale bar = 25 μm. **E–H.** Double immunostaining of TMRM-purified cardiomyocytes at Flk-d8 for connexin43 (Cx43) (green) and cTnT (orange) (E), Cav3.2 (green) and cTnT (orange) (F), HCN4 (green) and cTnT (orange) (G), Kir2.1 (green) and cTnT (orange) (H). Nuclei are visualized with DAPI. Scale bars = 25 μm. I. FACS analysis for cardiac progenitor induction from mouse iPSCs by CSA. X axis: CXCR4. Y axis: Flk1. Percentages of FCV cardiac progenitor cells (double positive population; red boxes) in total $Flk1^+$ cell progenies are indicated.
doi:10.1371/journal.pone.0016734.g001

Flowcytometry and cell sorting

FACS for differentiating mouse iPSCs was performed as described previously [8], [12], [20]. After 96–108 h of iPSC differentiation, cultured cells were harvested and stained with allophycocyanin (APC)-conjugated AVAS12 and FITC-conjugated ECCD2. Viable $Flk1^+$/E-cadherin$^-$ cells, excluding propidium iodide (Sigma), were sorted by FACS AriaII (Becton Dickinson). For FACS for FCV progenitor cells, after 2 days differentiation of purified $Flk1^+$ cell on PKH67-stained OP9 cells (Flk-d2), cultured cells were harvested and stained with a combination of MoAbs of PE-conjugated AVAS12 and biotinylated CXCR4 followed by addition of streptoavidin-conjugated APC, and subjected to FACS analysis. PKH-negative populations were analyzed and sorted as iPSC-derived cells. The $Flk1^+$/$CXCR4^+$ population (which was vascular endothelial cadherin-negative) [8] was designated "FCV cells". For FACS for cardiomyocytes, cells were harvested after 6–8 days culture of $Flk1^+$ cells on OP9 cells (Flk-d6-8). Induced cardiomyocytes were selected using tetramethyl rhodamine methyl ester (TMRM) (Invitrogen) [12], a fluorescent probe to monitor the membrane potential of mitochondria. In brief, cells were dissociated with 0.25% tryprin/EDTA, then incubated in DM with 50 nmol/L TMRM at 37°C for 15 minutes. Stained cells were washed twice and selected by FACS. TMRM-high population was considered as purified cardiomyocytes in iPSCs.

Human iPSC culture

END-2 cells were cultured as described previously [31]. Human iPS cell lines induced with transduction of four transcription factors (Oct4, Sox2, Klf4, and c-myc), 201B6 and 201B7, and Myc-negative human iPSC lines, 253G1 and 253G4 were maintained as previously described [1], [32]. 253G1 was used as the human iPS cell representative in all experiments unless stated otherwise. Induction of cardiomyocyte differentiation from human iPSCs was performed by co-culturing clumps of undifferentiated human iPSCs on END-2 cells, essentially as described previously [31]. To study the effect of CSA on cardiomyocyte differentiation, 3 μg/mL CSA was added to the culture medium on day 0 (END2-d0) or 8 (END2-d8) after start of co-culture. The number of beating colonies on END2-d12 was scored by microscopic examination. For intracellular Ca^{++} measurement and immunostaining for cTnT and actinin, beating colonies were mechanically excised, then gently dissociated by trypsin-EDTA treatment (at 37°C, 10 min), and replated on to gelatin-coated dishes. For electrophysiological analysis, beating colonies were mechanically excised and then dissociated by trypsin-EDTA with DNAse I (at 37°C, 10–15 min), and replated on to gelatin-coated dishes.

Immunohistochemistry

Immunostaining of murine cardiomyocytes was performed as described [8], [11], [12]. Briefly, 4% paraformaldehyde (PFA)-fixed cells were blocked by 2% skimmed milk (BD, bioscience) and incubated with 1st Abs. For immunohistochemistry, anti-mouse IgG –horse radish peroxidase (HRP) (Invitrogen) was used as 2nd Abs. For immunofluorescent staining, anti-mouse, rat and rabbit immunoglobulin conjugated with Alexa 488 or 546 were used for 2nd Abs. Nuclei were visualized with DAPI (Invitrogen). Cardiomyocyte differentiation was quantified as the fluorescent intensity of cTnT staining as described [8]. Immunostaining for human cardiomyocytes, 4% paraformaldehyde (PFA)-fixed cells were processed with 0.2% Triton X100 and 1% BSA (Sigma), and incubated with 1st Abs. Stained cells were photographed with inverted fluorescent microscopy, Eclipse TE2000-U (Nikon, Tokyo, Japan), digital camera system, AxioCam HRc (Carl Zeiss, Germany), or BIOREVO BZ-9000 (Keyence, Osaka, Japan).

Electrophysiology

Membrane potentials of single cells within a beating colony were measured using whole-cell patch clamp electrophysiology in the current-clamp mode (Axopatch200B, Axon Instruments/Molecular Devices Corp., Union City, CA). All recordings were carried out at room temperature [8].

Buffer compositions. Bath solution contained (in mmol/L) 140 NaCl, 5.4 KCl, 0.33 NaH_2PO_4, 0.45 $MgCl_2$, 1.8 $CaCl_2$, and 5 HEPES (pH = 7.4 with NaOH). Pipette solution contained (in mmol/L) 110 L-Aspartic acid, 30 KCl, 5 MgATP, 0.1 NaGTP, 5 K_2Creatine phosphate, 2 EGTA, 10 HEPES, and 10 NaOH (pH = 7.2 with KOH).

Field potential (FP) recordings of the beating colonies were performed using The MED64 multi-electrode array (MEA) system (Alpha MED Scientific Inc., Osaka, Japan) at a sampling rate of 20 kHz with low path filter of 500 Hz or high path filter of 1 Hz. All MEA measurements were performed at 37°C with heated perfusion system. The signals were recorded and processed with the Mobius software (WitXerx, US). The medium were perfused 1.7 ml/min as 37°C, and then the FPs were recorded for 5 min. Subsequently, E-4031(Calbiochem, US), isoproterenol (Proternol-L®, Kowa Pharmaceutical Company, Tokyo, Japan), or propranprol (Inderal®, AstraZeneca, Japan) was added to medium (discrete colony samples were used for each drug). Then, the FPs were measured for about 10 min.

Intracellular Ca measurement

Human iPSCs were loaded with 4 μM Quest Fluo-8 (ABD Bioquest, Inc. Sunnyvale, CA) for 30 min. Fluo-8 fluorescence (excitation at 495±10 nm and emission at 535±20 nm) of beating colony was measured every 16 msec with a back-thinned electron multiplier CCD camera (ImagEM; Hamamatsu Photonics, Hamamatsu, Japan). Four consecutive images were averaged. Ratio (F1/F0) to an image at minimum fluorescence intensity (F0) was calculated after background subtraction. The measurements were carried out at room temperature.

Reverse Transcription Polymerase Chain Reaction (RT-PCR)

Total RNA was isolated from various kinds of cell populations with the use of RNeasy Mini Kit (QIAGEN, Valencia, CA). cDNA was synthesized by the SuperScript III First-strand Synthesis System (Invitrogen). Polymerase chain reaction was performed with the use of KOD Plus (Toyobo, Tokyo, Japan) as described [33]. Primer sequences [34] are shown in Table S1.

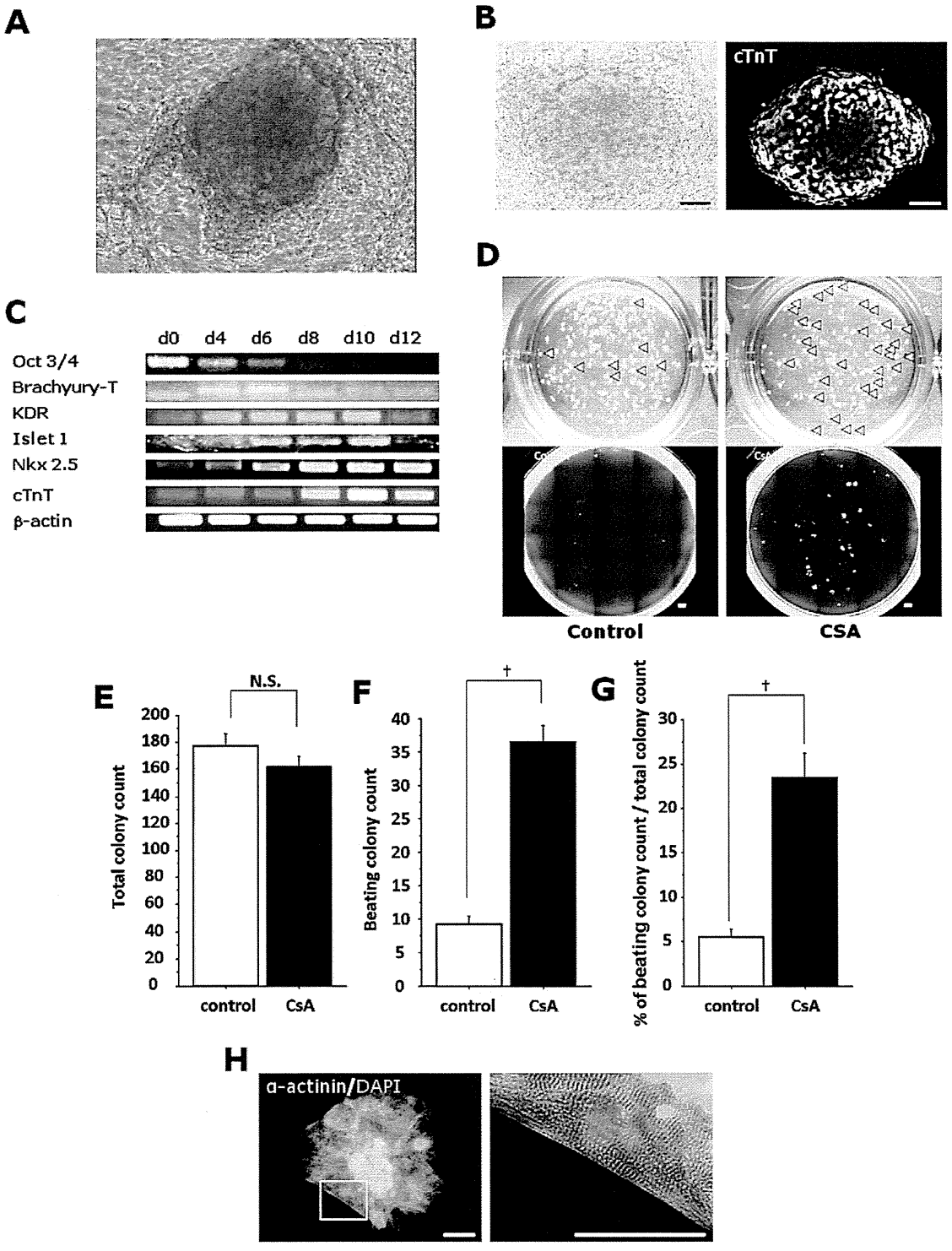

Figure 2. Induction and expansion of cardiomyocytes from human iPSCs. Human iPSCs were co-cultured with END-2 cells to differentiate cardiomyocytes. **A.** Gross morphology of a beating colony from human iPSCs (captured photo from Movie S1). **B.** cTnT staining of a beating colony on END-2 cells. Left panel: phase contrast image. Right panel: human cTnT staining (green). Scale bar = 50 μm. **C.** RT-PCR analysis for differentiation markers during cardiomyocyte differentiation of human iPSCs (from END2-d0 to d12). Oct3/4: Undifferentiated cell marker, Brachyury-T: mesendoderm marker, KDR (human Flk1): mesoderm marker, Islet1: mesoderm and cardiac progenitor marker, Nkx2.5: cardiac progenitor and cardiomyocyte marker, cTnT: cardiomyocyte marker. **D.** Representative gross appearance of human iPSC-derived beating colonies at END2-d12 in 12-well dishes. Left panels: control. Right panels: CSA treatment from END2-d8. Upper panels: phase contrast images. Beating colonies are shown by red arrows. Lower panels: cTnT staining (green). **E–G** Quantitative evaluation of beating colony appearance. **E.** Total colony count (control; 177±9.7/well (12-well dishes)(n = 8), CSA; 162±8.0/well (n = 9); N.S., p = 0.237), **F.** Beating colony count (control; 9.1±1.2/well (12-well dishes)(n = 8), CSA; 36.4±2.5/well (n = 9); †, $p<0.0001$), and **G.** Percentages of beating colonies (control; 5.4±0.9% (n = 8), CSA; 23.5±2.8% (n = 9); †, $p<0.0001$) in total colonies that appeared at END2-d12. **H.** Immunostaining of actinin (red) and DAPI (blue) in dissociated cardiomyocyte colonies. The same colony is shown in Movie S2. Right panel shows higher magnification of boxed area. Sarcomere structures are evident. Scale bar = 50 μm.
doi:10.1371/journal.pone.0016734.g002

Electron microscopic study

Human iPSC-derived beating colony was replated on multi-well chamber slide (NUNC Rochester, NewYork), fixed with 2% glutaraldehyde in 0.1 mol/L phosphate buffer (pH 7.4) for 30–60 min, washed and immersed with phosphate buffered saline for overnight at 4°C, and fixed in 1% buffered osmium tetroxide. The specimens were then dehydrated through graded ethanol and embedded in epoxy resin. Ultrathin sections (90 nm), double-stained with uranyl acetate and lead citrate, were examined under electron microscopy (H-7650; Hitachi, Tokyo, Japan).

Statistical Analysis

All data were obtained from at least three independent experiments. Statistical analysis of the data was performed using Student's t-test or ANOVA. $p<0.05$ was considered significant. All data are shown as mean ± S.D.

Results

Cardiomyocyte and cardiac progenitor expansion from mouse iPSCs by CSA

Recently, we reported that functional cardiomyocytes were induced from mouse iPSCs with our differentiation method in mouse ES cells [12]. In brief, undifferentiated mouse iPSC colonies maintained on MEFs were morphologically similar to mouse ESCs. We induced mesoderm differentiation from mouse iPSCs by culturing on type IV collagen-coated dish with DM (see Methods). $Flk1^+$ mesoderm cells that appeared were selected by FACS at 4.5 days of differentiation (iPS-d4.5) and then underwent a cardiomyocyte induction protocol involving co-culture on OP9 stroma cells; spontaneously beating cardiomyocytes began to appear after 3 to 4 days of culture (Flk-d3-4). Beating cells that appeared were positive for multiple cardiomyocyte markers and had electrophysiological features assessed by whole-cell patch clamp as previously reported [8], [12].

In the present study, we first tried to expand cardiomyocytes and cardiac progenitors from mouse iPS cells by CSA. When CSA was added to purified $Flk1^+$ cells, the appearance of $cTnT^+$ cardiomyocytes was increased 12-fold compared to controls (Fig. 1A, B), which was comparable with the increase observed in mouse ESCs [11]. CSA-expanded cardiomyocytes spontaneously beat and showed cardiomyocyte-like action potential (average interval: 0.74 sec, maximum diastolic potential: −58.6 mV and overshoot: 34.3 mV (n = 6)) (Fig. 1C). These cardiomyocytes also showed distinct sarcomere formation (Fig. 1D), expression of cTnT (Fig. 1E-H) and connexin 43 located at cellular boundaries (Fig. 1E). T-type calcium channel Cav3.2 (Fig. 1F), a pacemaker ion channel, HCN4 (Fig. 1G), and a ventricular ion channel, kir2.1 (Fig. 1H) were also detected in $cTnT^+$ cells. We also examined the effect of CSA on the induction of FCV cardiac progenitor cells in mouse iPSCs. Addition of CSA to $Flk1^+$ cells specifically increased the FCV population in mouse iPSCs to approximately 6.5 times of control. The maximum percentage of FCV cells within total $Flk1^+$ cell-derived cells was more than 30% by CSA (Fig. 1I), comparable with that observed in mouse ESCs, previously [11]. CSA can thus efficiently enhance the differentiation of functional cardiomyocytes and cardiac progenitors from mouse iPSCs.

Differentiation of cardiomyocytes from human iPSCs

We next examined cardiomyocyte differentiation from human iPSCs. We employed a human ESC differentiation method for cardiomyocytes using END-2 visceral endodermal stroma cells [31]. When human iPSCs were cultured on END-2 cells, spontaneously beating cardiomyocytes were successfully induced (Fig. 2A, Movie S1). Beating colonies were first detected after END2-d10 and became maximally evident after END2-d12.

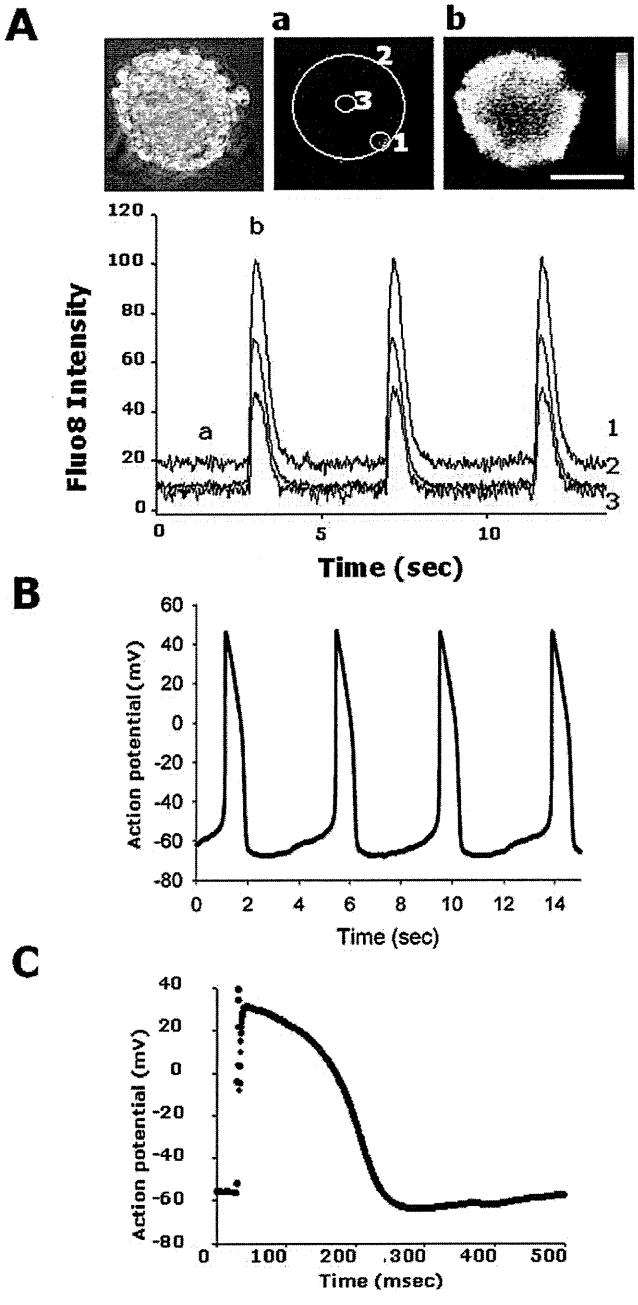

Figure 3. Functional analysis of expanded human cardiomyocytes. A. Ca^{++} transient in dissociated beating colonies. Cytoplasmic Ca^{++} change was monitored with fluo-8. Left panel: a transmission image of fluo-8 loaded iPSC colony. Middle and right panels: Fluo-8 images at the end (a) and the peak (b) of the fluorescence change. Scale bar = 50 μm. Lower panel: Time course of fluo-8 intensity change. The intensity was measured at the periphery (1), the entire colony (2) and the center (3) (ROIs shown in middle panel). Ratios (F1/F0) of the intensity to the one at the beginning of recording (F0) are indicated. Note that Ca transient is well synchronized within the colony. Real time video is shown in Movie S3. **B.** Representative action potential recorded from a cell in a beating colony. **C.** Representative single whole cell patch-cramp recording of a non-self beating human iPSC-derived cardiomyocyte after electrical stimulation.
doi:10.1371/journal.pone.0016734.g003

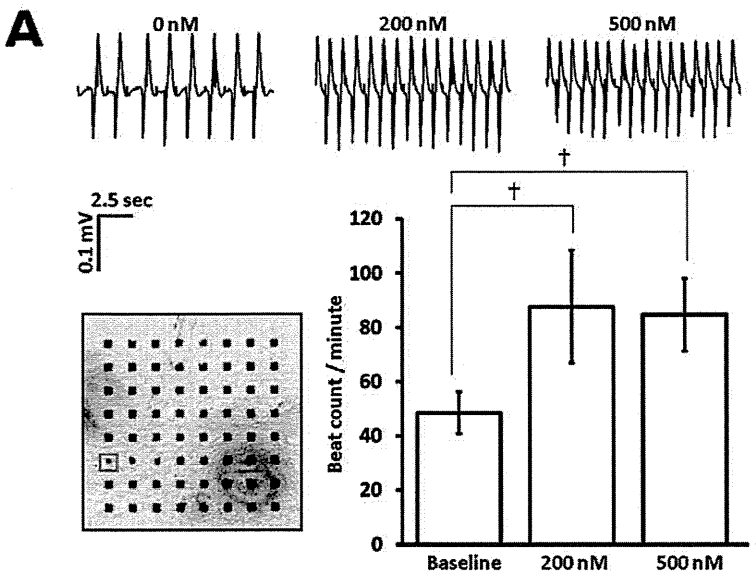
A
0 nM
200 nM
500 nM
2.5 sec
0.1 mV
Beat count / minute
120
100
80
60
40
20
0
Baseline
200 nM
500 nM
†
†

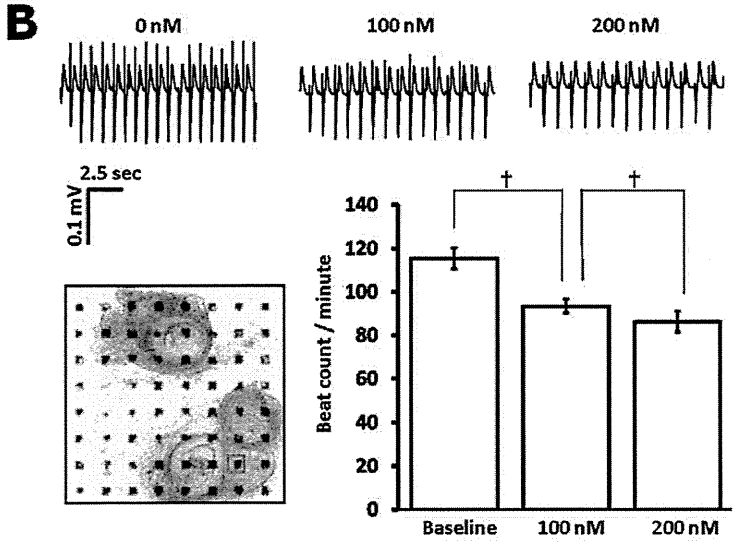
B
0 nM
100 nM
200 nM
2.5 sec
0.1 mV
Beat count / minute
140
120
100
80
60
40
20
0
Baseline
100 nM
200 nM
†
†

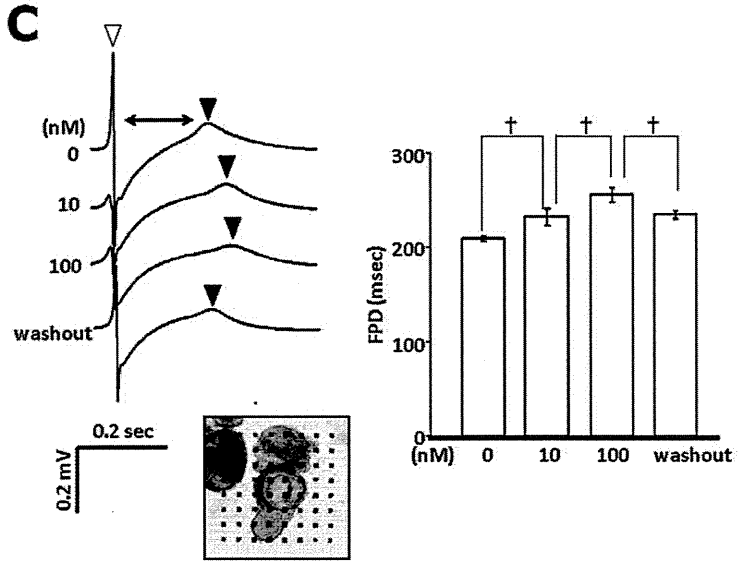
C
(nM)
0
10
100
washout
0.2 sec
0.2 mV
FPD (msec)
300
200
100
0
(nM) 0 10 100 washout
†
†
†

Figure 4. Pharmacological responses of human iPSC-derived cardiomyocytes. Field potential recordings of replated beating colonies after stimulation with isoproterenol (**A**), propranorol (**B**), and E-4031 (**C**). Photos; array of multi-electrode and replated colonies. Data recorded at electrodes in red squares are shown. **A, B.** Beating frequency (beating/minite). **C.** QT elongation. The time period from the first negative peak (open triangle) to the first positive peaks (closed triangles) reflects QT time in electrocardiogram. n = 3, †, $p<0.001$.
doi:10.1371/journal.pone.0016734.g004

These beating colonies were positive for cTnT (Fig. 2B). During the differentiation of human iPSCs on END2 cells, sequential expression of various marker genes expected for cardiomyogenesis was observed (ex: Oct3/4; undifferentiated iPSCs, Brachyury; mesendoderm, KDR; mesoderm, islet1; mesoderm and cardiac progenitors, nkx2.5; cardiac progenitors and cardiomyocytes, cTnT; cardiomyocytes) (Fig. 2C). In our another previous study on human ESC differentiation, a Flk1 (in human, VEGF receptor-2)$^{+}$/TRA1-60^{-} mesoderm population appeared in culture approximately 8 days after induction of differentiation [35]. When CSA was added to differentiating human iPSCs at the mesoderm stage (i.e. on END2-d8), the appearance of beating colonies was increased (Fig. 2D) although no effect was observed with the CSA treatment on undifferentiated human iPSCs (i.e. from END2-d0) (data not shown). Whereas the total number of iPSC-derived colonies that appeared was not changed (Fig. 2E), the number and percentage of beating colonies that appeared at END2-d12 were significantly increased approximately 4.0 and 4.3 times by CSA treatment, respectively (Fig. 2F, G). Approximately 23±2.7% of total colonies was beating in average, and in an optimized condition, 39% of total colonies included beating cardiomyocytes. CSA-expanded colonies maintained self-beating after a mechanical isolation and re-plating, and were positive for α-actinin with distinct sarcomere formation (Fig. 2H, Movie S2). Thus, cardiomyocyte induction from human iPSCs could be similarly enhanced by CSA. The mesoderm stage-specific effect of CSA in human iPSCs suggests the similar machinery in mouse ES/iPSCs are robustly working in human iPSC differentiation to cardiomyocytes.

Functional features of expanded human iPSC-derived cardiomyocytes

We next evaluated functional features of CSA-expanded human iPSC-derived cardiomyocytes. Fluo-8 imaging revealed synchronized increases in intracellular Ca^{++} in beating colonies with contraction (Fig. 3A, Movie S3). Action potentials recorded by patch clamp electrophysiology identified cells with pacemaker potential (average of the interval: 4.26 sec, maximum diastolic potential: −67.6 mV overshoot: 46.6 mV (n = 6))(Fig. 3B). Replated colonies continued beating spontaneously for more than 10 months. Some isolated single cells obtained from beating colonies at 3 months culture period lost automaticity and showed some features of human ventricular cells such as action potential with rapid depolarization and prolonged plateau after electrical stimulation (Fig. 3C). These results indicate that various functional human cardiomyocytes could be induced in this system.

We further examined pharmacological reactions of CSA-expanded human cardiomyocytes to show the relevance as cardiac cell models. We recorded field potential of re-plated beating colonies with multi-electrode array under simulation of a β-stimulant, isoproterenol, a β-blocker, propranorol, and a HERG channel inhibitor, E-4031. Addition of isoproterenol significantly increased the beating frequency (Fig. 4A), on the other hand, propranorol significantly decreased the beating frequency (Fig. 4B). E-4031 dose-dependently prolonged the length of time from the first negative peak to first positive peak, which is corresponding to QT time in electrocardiogram (Fig. 4C). These results indicate that CSA-expanded human iPSC-derived cardiomyocytes can suffice multiple functional features as human cardiomyocyte cell models.

Ultra structural features of expanded human iPSC-derived cardiomyocytes

We finally confirmed features of CSA-expanded human iPSC-derived cardiomyocytes at the ultrastructural level using electron microscopy. Beating colonies induced from human iPSCs resembled native cardiomyocytes, showing myofibrillar bundles with transverse Z-bands and enriched mitochondria (Fig. 5A-D). Other cardiomyocyte-specific structures, such as intercalated disks with desmosomes (Fig. 5D), atrial secretory granule-like structures (Fig. 5E), and glycogen granules (Fig. 5F) were also observed.

Together, these results indicate that *bona fide* human cardiomyocytes can be successfully induced and expanded from human iPSCs with this method.

Discussion

Here we demonstrated the induction and expansion of cardiac progenitors and functional cardiomyocytes from iPSCs using potent and specific effect of CSA. Human cardiomyocytes with multiple expected structural and functional features could be induced with this method. This method provides a critical technological basis to obtain cardiac cells from human iPSCs.

We have demonstrated previously that CSA treatment is most effective in inducing FCV cardiac progenitor cells, the nearest upstream of cardiomyocytes in mouse ESCs [11]. Here we showed that CSA effects on FCV cardiac progenitor and cardiomyocyte induction were also completely reproduced in mouse iPSCs. Moreover, CSA also showed significant enhancing effects of cardiomyocyte differentiation from human iPSCs in the END-2 system. This is the first report to show the effect of CSA in human stem cells. In this study, we examined four human iPSC clones, 201B6, B7 (induced with four factors) [1], 253G1 and G4 (induced without c-myc) [32]. Though the basal efficiency of cardiomyocyte differentiation from 201B6, B7 and 253G4 were lower than that from 253G1, CSA treatment significantly enhanced cardiomyocyte appearance similarly in all these human iPSC clones (Figure S1). Thus, CSA robustly induced cardiogenic differentiation in mouse ESCs, iPSCs and human iPSCs regardless their species and derivation methods.

The molecular mechanisms conducting this potent CSA effect on cardiac lineage is important, but still it is unknown. Though we examined another calcineurin inhibitor, FK506, and a NF-AT inhibitor, 11R-VIVIT, both of them did not reproduce the effect of CSA [11], indicating that the cardiogenic CSA effect is mediated by other molecular target than immunosuppressing effect of CSA. Further elucidation of molecular mechanisms of CSA in cardiomyocyte differentiation would be critical for the exploration of cardiomyocyte differentiation and regeneration strategies.

CSA-expanded cardiomyocytes from human iPSCs exhibited many features sufficing as functional cardiomyocytes. Cardiomyocytes with pacemaker-like or ventricular-like action potentials were successfully induced. Nevertheless, they were still immature compared with mature adult cardiomyocytes [36], [37] and they

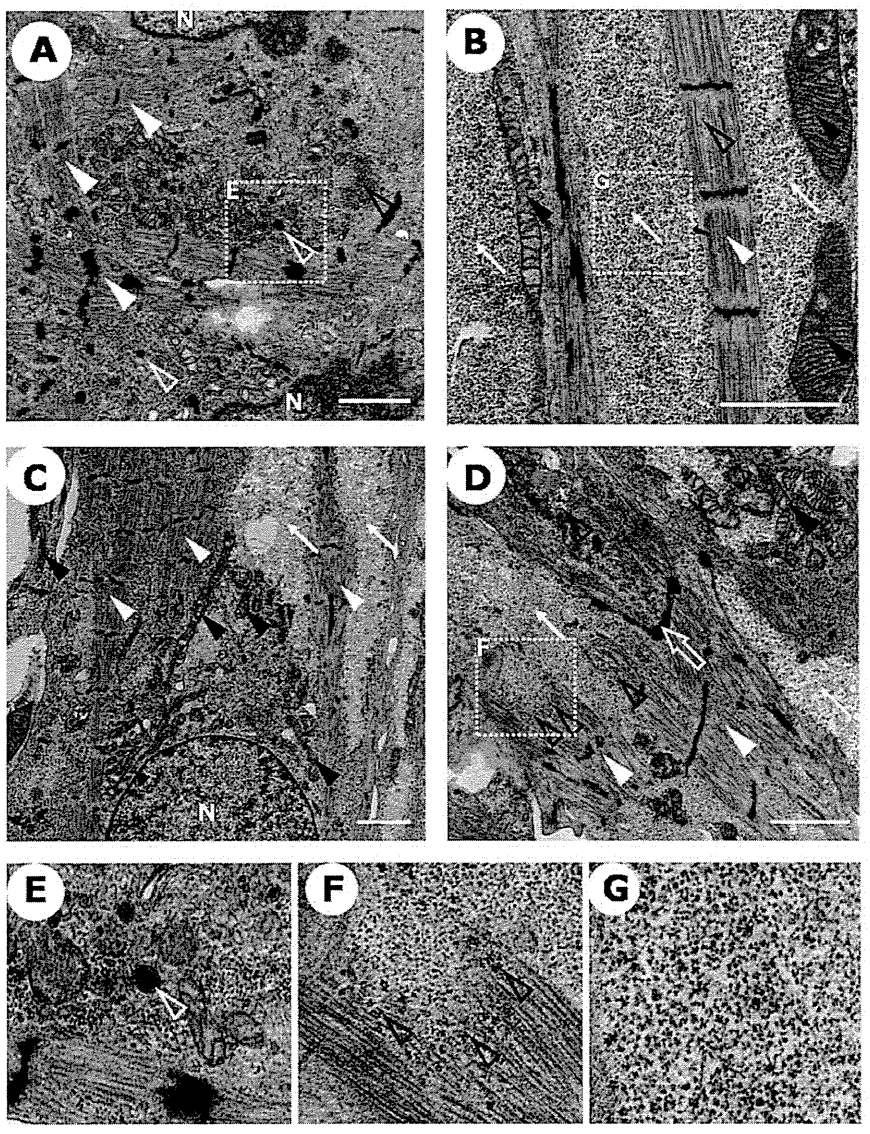

Figure 5. Ultrastructural analysis of human iPSC-derived cardiomyocytes. Transmission electron microscopic images of beating colonies. Myofibrils with Z-bands (white closed arrowheads in **A–D.**), mitochondria (black closed arrowheads in **B–D.**), intercalated disk-like structure with desmosome (white open arrow in **D.**), atrial sercetory granules (electron-dense granules surrounded by double membranes. White open arrowheads in **A.** and **E.** (magnified image of **A.**)), glycogen granules (electron-dense small granules. Black open arrowheads in **D.** and **F.** (magnified image of **D.**)), ribosomal granules (electron-lucent small granules. White arrows in **B–D.** and **G.** (magnified image of **B.**)). N: nucleus. Scale bar = 2 μm, direct magnify, ×3000 (A), ×7000 (B), ×4000 (C), ×5000 (D).
doi:10.1371/journal.pone.0016734.g005

also displayed some structural features of fetal cardiomyocytes, such as relatively low global electron density, sparse myofibrils, and abundant ribosome granules (Fig. 5). Methods for further maturation as well as specific induction and purification of the various cardiac cell types (pacemaker, atrial, ventricular, conduction system cells etc.) should be explored in future study.

Interestingly, a recent clinical report showed that CSA prevented cardiac reperfusion injury by protecting cardiomyocytes from apoptosis [38]. Cardiogenic effects of CSA in later stages of differentiation of human iPSCs imply that CSA may positively affect on endogenous cardiac progenitors to induce cardiac regeneration in patients. Though it is still unknown whether endogenous cardiac regeneration can be induced by CSA administration, our study may offer a scientific basis to support a clinical opportunity for CSA as a cardiac regenerative drug.

This novel cardiac cell differentiation method for iPSCs would thus broadly contribute to cardiac regenerative medicine by providing various options for cell preparation, transplantation strategies, and drug discovery.

Supporting Information

Figure S1 Quantitative evaluation of beating colony appearance in iPSC clones. 201B6 cells: Total colony count (control; 203±6.4/well (12-well dishes)(n = 3), CSA; 193±4.0/well (n = 3); N.S., p = 0.0915), beating colony count (control; 4.0±1.0/well (n = 3), CSA; 13.7±3.5/well (n = 3); *, $p<0.05$), percentages of beating colonies (control; 2.0±0.5% (n = 3), CSA; 7.1±1.7% (n = 3); **, $p<0.01$) in total colonies that appeared at END2-d12. 201B7 cells: Total colony count (control; 204±8.3/well (n = 3),

CSA; 200±2.0/well (n = 3); N.S., p = 0.43), beating colony count (control; 5.0±1.0/well (n = 3), CSA; 18.3±3.1/well (n = 3); **, p<0.01), percentages of beating colonies (control; 2.5±0.6% (n = 3), CSA; 9.2±1.5% (n = 3); **, p<0.01). 253G4 cells: Total colony count (control; 201±4.0/well (n = 3), CSA; 201±3.8/well (n = 3); N.S., p = 0.9216), beating colony count (control; 4.7±0.6/well (n = 3), CSA; 15.0±1.0/well (n = 3); **, p<0.05), percentages of beating colonies (control; 2.3±0.3% (n = 3), CSA; 7.5±0.6% (n = 3); †, p<0.001)
(TIF)

Movie S1 A beating colony induced from human iPS cells at END2-d12 (Fig. 2A).
(MOV)

Movie S2 A dissociated beating colony induced from human iPS cells on END-2 cells (Fig. 2H).
(MOV)

Movie S3 Real time monitoring of Ca^{++} transient by Fluo-8 in dissociated beating colony induced from human iPS cells (Fig. 3A). Clear and synchronized Ca^{++} transient is observed.
(MOV)

Table S1 Primers for PCR.
(RTF)

Acknowledgments

We thank Dr. D. Ward (Leiden University Medical Center) for supplying END-2 cells, Dr. G. Takemura (Gifu University Graduate School of Medicine) for interpretation and evaluation of electron microgram, Novartis Pharma for providing cyclosporin-A, Dr. M. Takahashi (Kyoto University Graduate School of Medicine) for critical reading of the manuscript.

Author Contributions

Conceived and designed the experiments: MF PY JKY. Performed the experiments: MF PY TGO GN HU HF HM SM. Analyzed the data: MF TI CLM JKY. Contributed reagents/materials/analysis tools: KO KT MN CLM. Wrote the paper: MF RS CLM NN KN SY JKY.

References

1. Takahashi K, Tanabe K, Ohnuki M, Narita M, Ichisaka T, et al. (2007) Induction of pluripotent stem cells from adult human fibroblasts by defined factors. Cell 131: 861–872.
2. Takahashi K, Yamanaka S (2006) Induction of pluripotent stem cells from mouse embryonic and adult fibroblast cultures by defined factors. Cell 126: 663–676.
3. Yamanaka S (2007) Strategies and new developments in the generation of patient-specific pluripotent stem cells. Cell Stem Cell 1: 39–49.
4. Nishikawa S, Goldstein RA, Nierras CR (2008) The promise of human induced pluripotent stem cells for research and therapy. Nat Rev Mol Cell Biol 9: 725–729.
5. Reinecke H, Minami E, Zhu WZ, Laflamme MA (2008) Cardiogenic differentiation and transdifferentiation of progenitor cells. Circ Res 103: 1058–1071.
6. Laflamme MA, Murry CE (2005) Regenerating the heart. Nat Biotechnol 23: 845–856.
7. Passier R, Oostwaard DW, Snapper J, Kloots J, Hassink RJ, et al. (2005) Increased cardiomyocyte differentiation from human embryonic stem cells in serum-free cultures. Stem Cells 23: 772–780.
8. Yamashita JK, Takano M, Hiraoka-Kanie M, Shimazu C, Peishi Y, et al. (2005) Prospective identification of cardiac progenitors by a novel single cell-based cardiomyocyte induction. FASEB J 19: 1534–1536.
9. Kattman SJ, Huber TL, Keller GM (2006) Multipotent Flk-1^+ cardiovascular progenitor cells give rise to the cardiomyocyte, endothelial, and vascular smooth muscle lineages. Dev Cell 11: 723–732.
10. Fukuda K, Yuasa S (2006) Stem cells as a source of regenerative cardiomyocytes. Circ Res 98: 1002–1013.
11. Yan P, Nagasawa A, Uosaki H, Sugimoto A, Yamamizu K, et al. (2009) Cyclosporin-A potently induces highly cardiogenic progenitors from embryonic stem cells. Biochem Biophys Res Commun 379: 115–120.
12. Narazaki G, Uosaki H, Teranishi M, Okita K, Kim B, et al. (2008) Directed and systematic differentiation of cardiovascular cells from mouse induced pluripotent stem cells. Circulation 118: 498–506.
13. Mauritz C, Schwanke K, Reppel M, Neef S, Katsirntaki K, et al. (2008) Generation of functional murine cardiac myocytes from induced pluripotent stem cells. Circulation 118: 507–517.
14. Schenke-Layland K, Rhodes KE, Angelis E, Butylkova Y, Heydarkhan-Hagvall S, et al. (2008) Reprogrammed mouse fibroblasts differentiate into cells of the cardiovascular and hematopoietic lineages. Stem Cells 26: 1537–1546.
15. Zhang J, Wilson GF, Soerens AG, Koonce CH, Yu J, et al. (2009) Functional cardiomyocytes derived from human induced pluripotent stem cells. Circ Res 104: e30–41.
16. Tanaka T, Tohyama S, Murata M, Nomura F, Kaneko T, et al. (2009) In vitro pharmacologic testing using human induced pluripotent stem cell-derived cardiomyocytes. Biochem Biophys Res Commun 385: 497–502.
17. Yokoo N, Baba S, Kaichi S, Niwa A, Mima T, et al. (2009) The effects of cardioactive drugs on cardiomyocytes derived from human induced pluripotent stem cells. Biochem Biophys Res Commun 387: 482–488.
18. Zwi L, Caspi O, Arbel G, Huber I, Gepstein A, et al. (2009) Cardiomyocyte differentiation of human induced pluripotent stem cells. Circulation 120: 1513–1523.
19. Moretti A, Bellin M, Jung CB, Thies TM, Takashima Y, et al. (2010) Mouse and human induced pluripotent stem cells as a source for multipotent $Isl1^+$ cardiovascular progenitors. FASEB J 24: 700–711.
20. Yamashita J, Itoh H, Hirashima M, Ogawa M, Nishikawa S, et al. (2000) Flk1-positive cells derived from embryonic stem cells serve as vascular progenitors. Nature 408: 92–96.
21. Nishikawa SI, Nishikawa S, Hirashima M, Matsuyoshi N, Kodama H (1998) Progressive lineage analysis by cell sorting and culture identifies $FLK1^+VE$-$cadherin^+$ cells at a diverging point of endothelial and hemopoietic lineages. Development 125: 1747–1757.
22. Kataoka H, Takakura N, Nishikawa S, Tsuchida K, Kodama H, et al. (1997) Expressions of PDGF receptor alpha, c-Kit and Flk1 genes clustering in mouse chromosome 5 define distinct subsets of nascent mesodermal cells. Dev Growth Differ 39: 729–740.
23. Yamashita J (2004) Cardiovascular cell differentiation from ES cells. In: Mori H, Matsuda H, eds. Cardiovascular Regeneration Therapies Using Tissue Engineering Approaches. Tokyo: Springer-Verlag GmbH, Chapter 2. pp 67–80.
24. Moretti A, Caron L, Nakano A, Lam JT, Bernshausen A, et al. (2006) Multipotent embryonic $isl1^+$ progenitor cells lead to cardiac, smooth muscle, and endothelial cell diversification. Cell 127: 1151–1165.
25. Wu SM, Fujiwara Y, Cibulsky SM, Clapham DE, Lien CL, et al. (2006) Developmental origin of a bipotential myocardial and smooth muscle cell precursor in the mammalian heart. Cell 127: 1137–1150.
26. Garry DJ, Olson EN (2006) A common progenitor at the heart of development. Cell 127: 1101–1104.
27. Yamashita JK (2007) Differentiation of arterial, venous, and lymphatic endothelial cells from vascular progenitors. Trends Cardiovasc Med 17: 59–63.
28. Yamashita JK (2004) Differentiation and diversification of vascular cells from embryonic stem cells. Int J Hematol 80: 1–6.
29. Yanagi K, Takano M, Narazaki G, Uosaki H, Hoshino T, et al. (2007) Hyperpolarization-activated cyclic nucleotide-gated channels and T-type calcium channels confer automaticity of embryonic stem cell-derived cardiomyocytes. Stem Cells 25: 2712–2719.
30. Okita K, Ichisaka T, Yamanaka S (2007) Generation of germline-competent induced pluripotent stem cells. Nature 448: 313–317.
31. Mummery C, Ward-van Oostwaard D, Doevendans P, Spijker R, van den Brink S, et al. (2003) Differentiation of human embryonic stem cells to cardiomyocytes: role of coculture with visceral endoderm-like cells. Circulation 107: 2733–2740.
32. Nakagawa M, Koyanagi M, Tanabe K, Takahashi K, Ichisaka T, et al. (2008) Generation of induced pluripotent stem cells without Myc from mouse and human fibroblasts. Nat Biotechnol 26: 101–106.
33. Yamamizu K, Kawasaki K, Katayama S, Watabe T, Yamashita JK (2009) Enhancement of vascular progenitor potential by protein kinase A through dual induction of Flk-1 and Neuropilin-1. Blood 114: 3707–3716.
34. Yang L, Soonpaa MH, Adler ED, Roepke TK, Kattman SJ, et al. (2008) Human cardiovascular progenitor cells develop from a KDR^+ embryonic-stem-cell-derived population. Nature 453: 524–528.
35. Sone M, Itoh H, Yamahara K, Yamashita JK, Yurugi-Kobayashi T, et al. (2007) Pathway for differentiation of human embryonic stem cells to vascular cell components and their potential for vascular regeneration. Arterioscler Thromb Vasc Biol 27: 2127–2134.
36. Chacko KJ (1976) Observations on the ultrastructure of developing myocardium of rat embryos. J Morphol 150: 681–709.
37. Kehat I, Kenyagin-Karsenti D, Snir M, Segev H, Amit M, et al. (2001) Human embryonic stem cells can differentiate into myocytes with structural and functional properties of cardiomyocytes. J Clin Invest 108: 407–414.
38. Piot C, Croisille P, Staat P, Thibault H, Rioufol G, et al. (2008) Effect of cyclosporine on reperfusion injury in acute myocardial infarction. N Engl J Med 359: 473–481.

Journal of Cardiology (2011) 57, 131–140

available at www.sciencedirect.com

ScienceDirect

journal homepage: www.elsevier.com/locate/jjcc

Review

Current biochemistry, molecular biology, and clinical relevance of natriuretic peptides

Toshio Nishikimi (MD, PhD, FJCC)*, Koichiro Kuwahara (MD, PhD), Kazuwa Nakao (MD, PhD)

Department of Medicine and Clinical Science, Kyoto University Graduate School of Medicine, 54, Shogoin-Kawara-cho, Sakyo-ku, Kyoto 606-8507, Japan

Available online 5 February 2011

KEYWORDS
Atrial natriuretic peptide;
Brain (B-type) natriuretic peptide;
C-type natriuretic peptide;
Heart failure

Summary The mammalian natriuretic peptide family consists of atrial (ANP), brain [B-type; BNP] and C-type natriuretic peptide (CNP) and three receptors, natriuretic receptors-A (NPR-A), -B (NPR-B) and -C (NPR-C). Both ANP and BNP are abundantly expressed in the heart and are secreted mainly from the atria and ventricles, respectively. By contrast, CNP is mainly expressed in the central nervous system, bone and vasculature. Plasma concentrations of both ANP and BNP are elevated in patients with cardiovascular disease, though the magnitude of the increase in BNP is usually greater than the increase in ANP. This makes BNP is a clinically useful diagnostic marker for several pathophysiological conditions, including heart failure, ventricular remodeling and pulmonary hypertension, among others. Recent studies have shown that in addition to BNP-32, proBNP-108 also circulates in human plasma and that levels of both forms are increased in heart failure. Furthermore, proBNP-108 is *O*-glycosylated and circulates at higher levels in patients with severe heart failure. In this review we discuss recent progress in our understanding of the biochemistry, molecular biology and clinical relevance of the natriuretic peptide system.

Contents

* Corresponding author. Tel.: +81 75 751 4287; fax: +81 75 771 9452.
E-mail addresses: nishikim@kuhp.kyoto-u.ac.jp, nishikim@dokkyomed.ac.jp (T. Nishikimi).

0914-5087/$ – see front matter
doi:10.1016/j.jjcc.2011.01.002

Introduction

The natriuretic peptide system consists of three distinct endogenous peptides: atrial natriuretic peptide (ANP), brain (or B-type) natriuretic peptide (BNP) and C-type natriuretic peptide (CNP), as well as three receptors: natriuretic peptide receptor-A (NPR-A or guanynyl cyclase-A), natriuretic peptide receptor-B (NPR-B or guanynyl cyclase-B) and natriuretic peptide receptor-C (NPR-C or clearance receptor). Recent advances suggest that through its pleiotropic effects, this system plays key roles in the regulation of blood pressure and body fluid volume. In this review, we discuss the current understanding of the biochemistry, molecular biology and clinical relevance of natriuretic peptides.

Structures of the genes and peptides

ANP

Kirsch reported in 1956 that mammalian atrial myocytes contain granules with morphologies similar to the granules found in endocrine cells [1]. However, the significance of these granules was not recognized until 1981, when de Bold et al. reported that intravenous injection of crude myocardial extract induces a natriuretic effect in rats [2], suggesting the heart contains a natriuretic hormone. These findings ultimately led to the identification of the complete amino acid sequence of ANP in mammalian atrial tissue [3]. Subsequent studies showed that ANP is synthesized and secreted from the heart into the circulation as a cardiac hormone in response to atrial stretch. The major molecular form of circulating ANP is a 28-amino acid peptide (α-ANP) with a ring structure formed by an intramolecular disulfide linkage (Fig. 1).

ANP gene contains three exons. Exon 1 encodes the 5′-untranslated region, a 25-amino acid signal peptide and the first 16 amino acids of proANP. Exon 2 encodes most of the proANP sequence, and exon 3 encodes the terminal tyrosine and 3′-untranslated region (Fig. 2). ANP mRNA is translated to 151-amino acid preproANP. Thereafter, the 25-amino acid signal peptide is removed, yielding 126-amino acid proANP (γ-ANP) [4]. Because the tissue molecular form of ANP in the atrium and ventricle is proANP, it is presumed that the proteolytic conversion of proANP to ANP occurs during secretion. Consistent with that notion, a recent study showed that a transmembrane enzyme, corin, cleaves proANP into α-ANP and N-terminal proANP [5]. Interestingly, human β-ANP, the antiparallel dimer of α-ANP, is also isolated from the human failing heart, and levels of β-ANP are increased in the myocardium [6] and plasma [7] in cases of severe heart failure (Fig. 2).

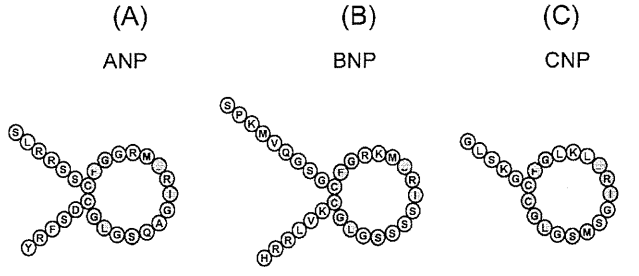

Figure 1 Structures of the human natriuretic peptide family members: (A) ANP; (B) BNP; and (C) CNP. Identical amino acids sequences are indicated by yellow shading.

BNP

BNP was first isolated from porcine brain extracts in 1988 by Sudoh et al. [8]. Soon after its discovery, however, the highest concentrations of BNP were shown to be in the heart, where it acts as a cardiac hormone [9]. BNP peptides and cDNA clones from a variety of species have now been isolated and sequenced. The predominant circulating form of BNP is a 26-, 45- and 32-amino acid peptide in pig, rat and human, respectively [10]. Thus, whereas the structure of ANP is relatively well conserved among species, the structure of BNP differs. The mature active molecular form of human BNP is BNP-32 (Fig. 1). Like ANP gene, BNP gene contains three exons (Fig. 3). Exon 1 encodes a 26-amino acid signal peptide and the first 15 amino acids of proBNP. Exon 2 encodes most of the proBNP sequence, and exon 3 encodes the terminal tyrosine and the 3′-untranslated region. BNP mRNA is translated to 134-amino acid preproBNP, after which the 26-amino acid signal peptide is removed, yielding 108-amino acid proBNP-108. In contrast to ANP, atrial and ventricular tissue contain two molecular forms of BNP: proBNP-108 and BNP-32. BNP-32 is dominant (~60%) in atrial tissue, while

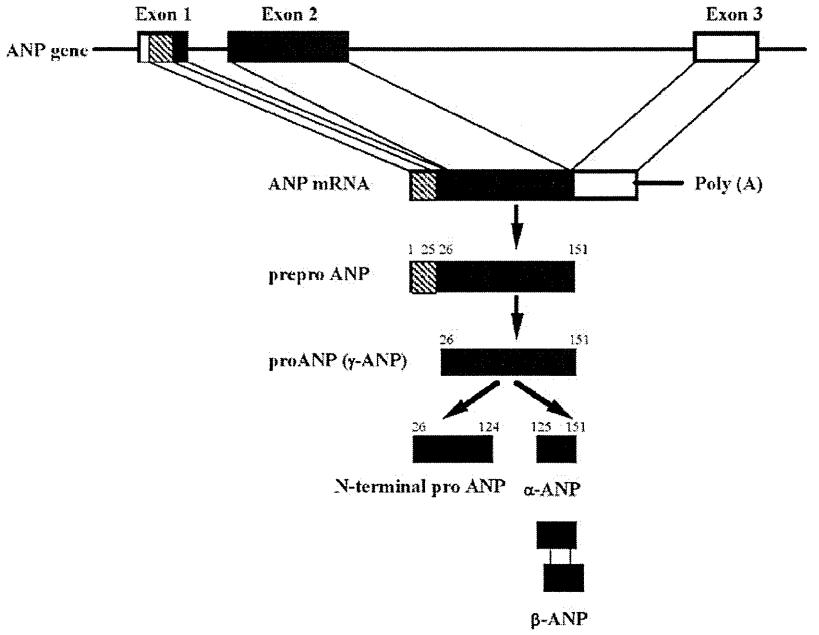

Figure 2 Structure of the gene and biosynthetic pathway of human ANP. mRNA: messenger RNA.

proBNP-108 is dominant (~60%) in ventricular tissue [11]. It is thought that cleavage of proBNP into BNP-32 and N-terminal proBNP-76 occurs in the trans-Golgi network [12] and that BNP-32 and N-terminal proBNP are then released into the circulation via a constitutive pathway. However, recent studies have shown that proBNP-108 is also present in human plasma and that the proBNP-108/BNP-32 ratio is increased in cases of severe heart failure [11]. We discuss the molecular forms of plasma BNP in detail in "Molecular complexity of plasma BNP — increase of proBNP-108 in heart failure" and "A new hypothesis of processing of proBNP" sections.

CNP

CNP was first isolated from porcine brain in 1990 [13]. Composed of 22 amino acids, the ring structure of CNP is highly homologous with those of ANP and BNP, but CNP uniquely lacks the carboxy-terminal extension (Fig. 1). Based on molecular cloning of CNP cDNA and the genes from various species, it has been predicted that the structure of CNP is identical among species and is the most highly conserved in the natriuretic peptide family. CNP-53, which has an amino-terminal extension of 31 amino acids, is a second endogenous form of CNP. Also first isolated from the porcine brain, CNP-53 has now been identified in both human and rat brain.

Like the other natriuretic peptide genes, CNP gene contains three exons. Exon 1 encodes a 23-amino acid signal peptide and the first 7 amino acids of proCNP. Exon 2 encodes the rest of the proCNP sequence, and exon 3 encodes the 3′ untranslated region (Fig. 4). PreproCNP is comprised of 126 amino acids, the first 23 of which are cleaved as a signal peptide. The resulting 103-amino acid proCNP is further processed to CNP-53 and/or CNP, the potencies of which

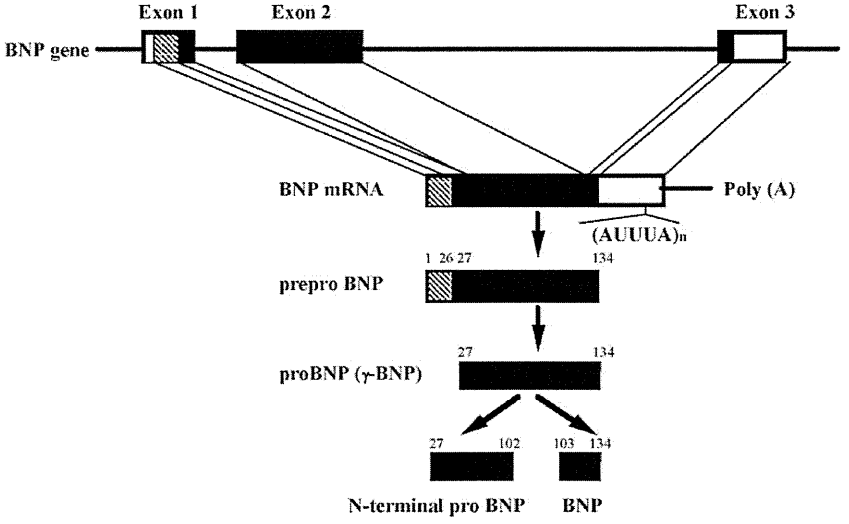

Figure 3 Structure of the gene and biosynthetic pathway of human BNP. mRNA: messenger RNA.